Highlight Review

Design, Synthesis, and Performance of NTA-modified Lipids as Templates for Histidine-tagged Protein Crystallization

David H. Thompson,* Mingkang Zhou, Jessica Grey, and Hee-kwon Kim

(Received May 22, 2007; CL-078005)

Abstract

Current methods of drug discovery and development typically involve either structure-based drug design approaches or high-throughput screening methods for lead identification. The structure-based discovery process relies heavily upon the labor-intensive determination of three-dimensional protein structures using X-ray diffraction (XRD) and NMR techniques. Although tens of thousands of soluble protein structures have been resolved at the atomic level using these methods, there are many drug targets, particularly integral membrane proteins, whose structures have not been elucidated. In the case of XRD, this limitation often arises from the lack of reliable and predictable methods for protein crystallization. The extensive number of proteins crystallized by the interfacial templating approach suggests that this method may offer great promise for structural biology applications, particularly for proteins that do not readily form X-ray quality crystals from bulk solution. This review highlights the various approaches that have been used for templating of protein crystallization at gas–liquid and solid–liquid interfaces. Special emphasis is placed on the synthesis of NTA- and IDA-conjugated lipids, their use in templating and concentrating proteins at lipid monolayer interfaces, and protein structure elucidations that have been facilitated by these metal-chelating lipids. Current approaches to control the nucleation and growth of protein crystals involving microfluidics, dip pen nanolithography, and non-covalent symmetry-based templating approaches are also discussed. Taken together, the progress in this field suggests that the interfacial templating approach to crystallization can develop into a powerful tool for high-throughput structural analysis by providing a universal, readily controllable method for crystallizing proteins.

List of abbreviations: biotin-DPPE, *N*-biotin-1,2-dipalmitoyl-3-phosphoethanolamine; CTAB, cetyltrimethylammonium bromide; DDAB, ditetradecyldimethylammonium bromide; DLPC, 1,2-dilauroyl-3-phosphocholine; DMPC, 1,2-dimyristoyl-3-phosphocholine; DNP-PE, *N*-dinitrophenylphosphatidylethanolamine; DOPC, 1,2-dioleoyl-3-phosphocholine; DOPE, 1,2-dioleoyl-3-phosphoethanolamine; DOPG, 1,2-dioleoyl-3-phosphoglycerol; DOPS, 1,2-dioleoyl-3-phosphoserine; DPPC, 1,2-dipalmitoyl-3-phosphocholine; DPPE, 1,2-dipalmitoyl-3-phosphoethanolamine; EPC, mixture of phosphatidylcholine lipids extracted from egg; erythrocyte Gb3, globoside 3 extracted from erythrocytes; GalCer, galactosyl ceramide; IDA, iminodiacetic acid; IMAC, immobilized metal affinity chromatography; lysoPC, 1-alkanoyl-3-phosphocholine; NTA, nitrilotriacetic acid; PC, phosphatidylcholine; SOPC, 1-stearoyl-2-oleoyl-3-phosphocholine; TEM, transmission electron microscopy; TR-DPPE, N-Texas Red-1,2-dipalmitoyl-3-phosphoethanolamine.

♦ Introduction

Structure-based design and high-throughput screening methods are the two most commonly used approaches for discovering new pharmaceutical leads. The screening approach involves the production and testing of thousands of compounds using an appropriate cell type or disease model to assess bioactivity. Once a lead compound is discovered, libraries of structurally related compounds are then synthesized and tested for their abilities to optimize the therapeutic effect and minimize side effects. One of the most successful examples of this approach is ivermectin, an antihelmintic that was discovered during a massive screening program at Merck in 1975.[1,2] The alternate approach involves the rational design of drugs such as *imatinib*[3] (the tyrosine kinase inhibitor for treatment of chronic myelogenous leukemia known as Gleevec) or zanamivir[4,5] (the neuraminidase inhibitor for treatment of influenza virus A & B known as Relenza). This method is based on a detailed structural knowledge of the drug target, which enables rapid optimization when combined with computer-aided design and/or structural elucidation of drug:target complexes. Given the labor-intensive nature of both methods, it is not surprising that the average total investment required for a new drug to advance from discovery to FDA approval is now more than $800 million dollars. Because of the rapid rise in drug discovery and development costs, the need for new tools to streamline this process is clear.

When the drug target is a macromolecule such as a protein, the most useful methods of structure determination are X-ray crystallography and NMR. Both techniques have been applied to solve many three-dimensional protein structures at atomic resolution; however, they both have practical limitations. X-ray crystallography is the most widely used and cost-effective tool for determining the atomic structures of proteins. By combining the electron density map obtained from X-ray diffraction patterns of high quality protein crystals with the known amino acid sequence, it is possible to deduce the three-dimensional structure of the protein. A significant challenge in protein crystallography is the computation of the atomic positions of thousands of atoms in the protein from the observed positions and intensities of the diffracted X-ray beam. Although this analysis has been greatly facilitated by the use of high-speed computers, the ultimate resolution of the protein structure is usually determined by the quality of the protein crystal.

Unlike X-ray crystallography, NMR spectroscopy utilizes highly concentrated protein solutions (ca. 1 mM) instead of well-ordered crystals. Methods such as 2D Nuclear Overhauser Enhancement Spectroscopy (NOESY) are used to observe inter-

Profs. David H. Thompson, Mingkang Zhou, Jessica Grey, and Hee-kwon Kim*
Department of Chemistry, Purdue University, 560 Oval Drive
Tel: 765-494-0386; FAX: 765-496-2592; E-mail: davethom@purdue.edu

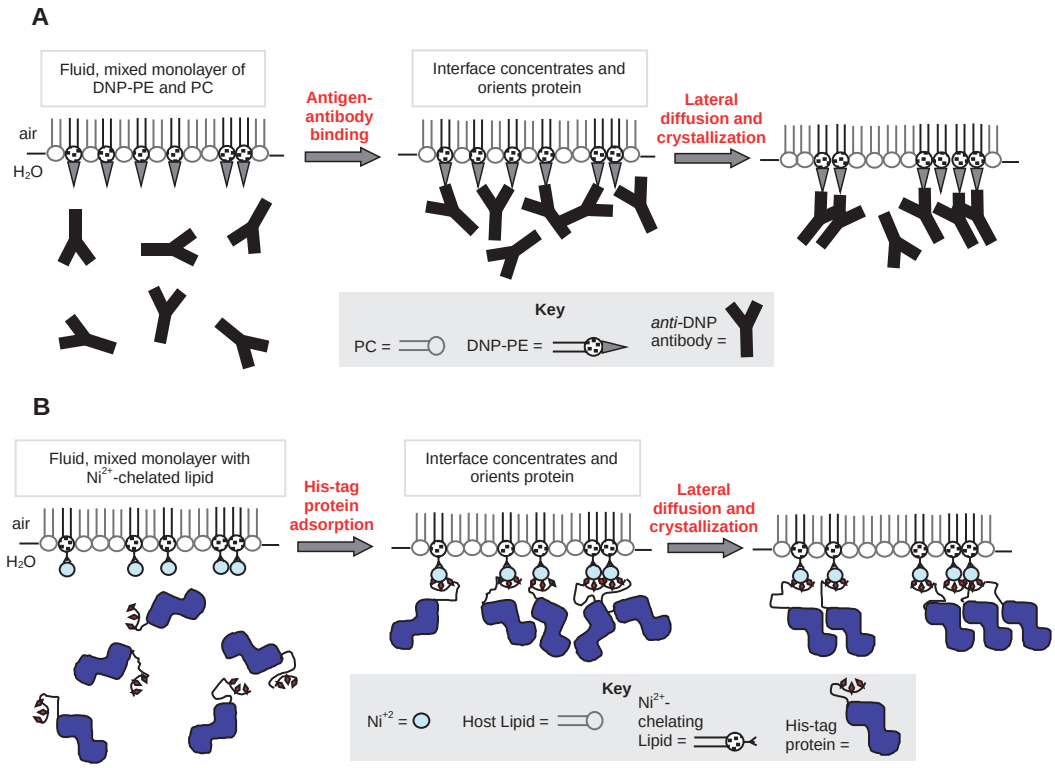

Figure 1. Conceptual diagram of 2D protein crystallization. The original Uzgiris and Kornberg concept (A) used an antigenic lipid, DNP-PE, to promote the adsorption of *anti*-DNP antibodies onto a mixed monolayer of 1:1 DNP-PE:PC. Hybridization of this concept with the principle of immobilized metal affinity chromatography produces an engineered interaction with the interface via his-tag:M^{n+}:NTA–lipid (or IDA–lipid) chelation (B).

actions between hydrogen atoms in the polypeptide chain that are close together (less than 5 Å apart). Proteins labeled with ^{15}N- and ^{13}C-enriched amino acids are used to resolve overlapping peaks in multi-dimensional NOESY spectra. By combining a large number of NOE proximity relationships with knowledge of the protein sequence, the three-dimensional conformation of the protein can be deduced. In most cases, however, the practical limit for protein structure determination of soluble proteins via NMR is approximately 30 kD.

Although there are tens of thousands of protein structures known at atomic resolution, there are many drug targets, particularly membrane proteins, whose structures are not known in sufficient detail to enable structure-based drug design. Unfortunately, protein crystal structures are not easily obtained, largely due to the lack of predictable and reliable methods for their crystallization. Compounding this problem is the fact that most proteins (1) display complex phase diagrams,[6–8] (2) are highly sensitive to solution conditions (e.g., pH, salinity, temperature, etc), (3) are difficult to obtain in highly pure form due to proteolytic degradation and occult impurities, (4) have a high degree of conformational flexibility that can produce misfolded states, (5) are difficult to concentrate under mild conditions, and (6) typically yield crystals that are fragile due to their high water content.

Protein crystals are grown from supersaturated solutions of the protein. Supersaturation is usually induced by the addition of inorganic salts (e.g., $(NH_4)_2SO_4$, NaCl, KCl, $CaCl_2$, etc.), volatile organic solvents (e.g., ethanol, acetone, acetonitrile, etc.), or polymers (e.g., polyethylene glycol (PEG)) as precipitants to a concentrated solution of the protein (Table 1). Discovery of the conditions necessary for the nucleation and growth of a well-ordered protein crystal is often an Edisonian process whereby each adjustable experimental variable such as pH, temperature, ionic strength, precipitant type, precipitant concentration, and humidity is changed systematically across a wide parameter space using different crystallization methods (Table 2). In general, the highest quality crystals are produced when the nucleation and crystal growth steps are kinetically well

Table 1. Methods for supersaturating protein solutions to induce their crystallization (adapted from Ref. 6)

1	Direct mixing of a precipitant with the protein to immediately create a supersaturated solution (batch method)
2	Lower (or raise) temperature
3	Raise (or lower) salt concentration
4	Change solution pH
5	Change the solubility of the protein by adding a ligand, removing a solubilizing agent or altering the dielectric of the solution
6	Concentrate the protein by removing water via evaporation
7	Add PEG or another polymer that produces an excluded volume in solution
8	Add an effector or a crosslinking agent such as a protein-specific antibody

Published on the web (Advance View) July 25, 2007; doi:10.1246/cl.2007.956

Table 2. Techniques used to induce protein crystallization (adapted from Ref. 6)

1	Batch method crystallization by precipitant addition (see Table 1)
2	Bulk evaporation (see Table 1)
3	Dialysis to slowly remove solubilizing agent or infuse precipitant
4	Immiscible liquid bridge between two miscible phases or free interface diffusion
5	Vapor diffusion from sessile drop
6	Vapor diffusion from hanging drop
7	Sequential extraction
8	Temperature-induced crystallization

separated.[8] The conditions for crystallizing related proteins are often similar, but can have their own unique requirements. As a consequence, some proteins readily crystallize, some do so only after much effort has been expended to discover the right conditions, while others never crystallize. Because water-insoluble integral membrane proteins (IMP) do not readily form crystals, only a few membrane proteins (ca. 130) have been crystallized and structurally characterized.

Significant barriers to rapid protein structure elucidation still exist. For example, X-ray methods require large amounts of pure protein to enable the screening of many different crystallization conditions to discover those that are capable of producing large ($>10\,\mu m$/side), high-quality single crystals. Since the phase diagram of the protein is typically unknown, most crystallization trials produce aggregates of amorphous protein phase, precipitates, or microcrystalline showers instead of single well-ordered crystals. Automated high-throughput screening methods[9–11] that utilize small quantities of protein solution ($0.1\,\mu L$) in a multi-well plate format are now commonly used for crystallization trials. This helps relieve the burden of large-scale expression and purification procedures when the protein is labile or in short supply. Microfluidic platforms have also been used to further reduce the volumes needed into the $\leq 10\,nL$ range.[12–15] The "sparse matrix" approach,[16,17] a searching strategy utilizing a limited set of extreme conditions in crystallization trials to rapidly discover the range of productive conditions and/or determine whether the IMP "wants" to crystallize, is another method that has been used. Once an initial "hit" has been identified via sparse matrix searching, further improvements in crystal size and quality are then achieved using a progressively narrower set of iterative searches around the original conditions. Other strategies used include (1) osmotic second virial coefficients (B_{22}) to determine the "crystallization slot"[18–22] where the experimentally determined B_{22} values lie in a window between -8×10^{-4} and $-2 \times 10^{-4}\,mol/g^2$, (2) "relative crystallizability" which describes the percentage of the crystal nucleation phase area within the protein and precipitating agent concentration ranges,[23] and (3) the crystallization coefficient (ξ_c, which is proportional to the ratio between the volume diffusion rate and the surface integration rate) to determine the "kinetic crystallization window" where $1 < \xi_c < 8$ for crystals grown at the air–water interface.[24]

Once a protein has been successfully crystallized, high-resolution 3D structural analysis by X-ray diffraction may still take many years. If the protein cannot be crystallized using any of these strategies, it must be expressed and purified in multiply labeled forms using ^{15}N- and ^{13}C-modified amino acids in sufficient amounts to facilitate NMR analysis. Consequently, a bottleneck exists in the determination of high-resolution protein structures due to the combined effect of these challenges. These limitations underscore the compelling need for new approaches in the structural biologist's repertoire.

♦ *Interfacial Templating Concept*

Overview

Crystallization of proteins from bulk solution requires that they become ordered with respect to nearest neighbor molecules and pack into a crystal lattice that may display low symmetry. This is difficult to achieve when the molecules possess highly convoluted topologies with irregular surface charge densities, are experiencing thermally excited internal dynamics that vary those surface features and properties, have no net orientation, and are undergoing Brownian motion in three dimensions. Interfacial templating approaches have been developed to address the last two issues by orienting the protein with respect to the interface and limiting the diffusion of the protein along it. One-dimensional (1D) and two-dimensional (2D) interfaces have been used to achieve these goals. Lamellar phases, lipid monolayers, and cubic phases have been used for two-dimensional crystallization of both soluble and membrane proteins (see below). They offer the advantage of providing large surface areas for protein adsorption, can be utilized with a wide variety of lipid conjugates to provide specific binding interactions, and can be made compatible with microfluidic interfaces. The disadvantage of this approach is that protein crystals grown at 2D interfaces may be only a single molecular layer in thickness. This makes them extremely challenging for analysis by conventional X-ray crystallographic methods. If the 2D crystals are analyzed by tilt-series electron crystallography, the reconstructed volume of the protein suffers from the "missing cone" problem due to the practical limitations of projecting the transmission electron microscope (TEM) beam through the sample stage at high tilt angles (i.e., protein structural information is lost when the stage tilt angle is $>57^\circ$ such that the electron beam can no longer pass through the sample). One-dimensional substrates have the advantage that proteins crystallized on their surface can be analyzed by helical reconstruction. This method, however, requires stringent control of the 1D substrate diameter, which can be difficult to achieve with most practical 1D substrates.

Two-dimensional Protein Crystallization at Lipid Monolayer Interfaces

The first step of monolayer-based 2D crystallization is the production of a planar lipid monolayer film at the air–water interface. This is achieved by spreading a solution of the desired lipids in a volatile organic solvent across the surface of an aqueous solution in a Langmuir trough. When the solvent evaporates, the lipids form a monolayer at the air–water interface, such that their polar headgroups are in contact with the aqueous phase and their nonpolar hydrocarbon chains are oriented toward the air where they can encounter the alkyl chains of neighboring lipids. The monolayer film can then be compressed

to generate a 2D gas-, fluid-, or solid-state film at the air–water interface.

If the protein of interest is present in the aqueous subphase below the monolayer film, it can become concentrated at the surface of the Langmuir trough if it possesses an affinity for the lipids at the air–water interface. The general operating principle in the 2D protein crystallization strategy, therefore, is the creation of surfaces that will specifically adsorb proteins present in the aqueous subphase, yielding >100-fold enrichments in protein concentration at the lipid interface. The combined effects of (1) elevated protein concentration, (2) enhanced protein alignment (relative to the freely tumbling solution state), and (3) fluid monolayer film properties to enable protein–protein interactions via lateral diffusion all contribute to the formation of 2D protein crystals. One of the first challenges in the interfacial crystallization approach, therefore, is the design of a lipid interface that bears a specific affinity interaction with the protein of interest. An additional design issue is the creation of dynamic (i.e., fluid) lipid interfaces that confer sufficient lateral and rotational mobility of the bound protein to enable optimization of intermolecular contacts and efficient packing into a crystalline array.[25–28]

There are several benefits that the 2D crystallization approach offers, such as simple experimental protocols and readily varied monolayer parameters that influence the crystallization process. The greatest advantage, however, is that 2D crystals grown at the air–water interface enable structural determination of the protein by negative-stain or cryo-transmission electron microscopy techniques, which are comparatively rapid and require only small amounts of material (10–1000 μg) relative to bulk crystallization screening methods.[29] Several successful examples of this technique are briefly summarized below.

♦ Experimental Approaches for Concentrating and Orientating Proteins at Lipid Monolayer Interfaces

The use of lipid monolayers as templates for 2D protein crystallization was first demonstrated by Uzgiris and Kornberg[30] in 1983. This seminal paper described the use of antigen–antibody interactions at the air–water interface to promote two-dimensional crystallization of anti-DNP IgG via complexation of DNP-modified phosphatidylethanolamine in a mixed monolayer of 1:1 DNP-PE and PC (Figure 1A). Even though the IgG structure reported was of low resolution, the flexibility and speed of the method led to further evolution of the technique using other types of lipid monolayer–protein interactions.

Electrostatic Adsorption

Kornberg and co-workers later used cationic lipids to electrostatically orient RNA polymerase II[31–33] for structural characterization by TEM. This approach ultimately enabled the determination of a 2.8 Å[34] structure by seeding the growth of 3D RNA pol II crystals using 2D crystals grown on cationic mixed lipid monolayers.[35] The electrostatic adsorption method has not been widely used for crystallization of other proteins since they often contain multiple patches of surface charge sites that would promote adsorption in multiple orientations at the monolayer interface in a pH- and ionic strength-dependent manner.

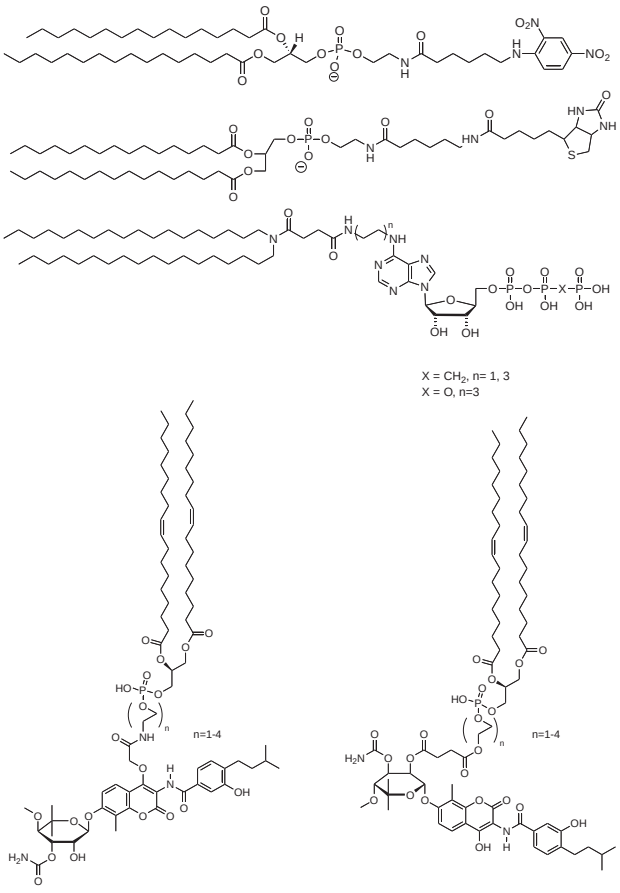

Figure 2. Ligand–lipid conjugates synthesized for ligand-specific protein immobilization and crystallization.

Biotin–Streptavidin and Other Specific Ligand–Protein Interactions

These landmark papers were followed by a host of related approaches using high affinity ligand–protein interations at the lipid–water interface. Kornberg and co-workers showed that streptavidin[36] will form 2D crystals at phosphatidylcholine monolayer air–water interfaces containing 2.3 mol % biotinylated lipids when the surface pressures were maintained at 25–30 mN/m. Electron microscopy studies of the 2D crystals grown from these interfaces revealed that the preferred growth direction is along one of two intersecting rows of intermolecular contacts. Further refinements of the biotinylated lipid–streptavidin method were later reported.[37–41] Several examples followed using new ligand–lipid conjugates that were synthesized to enable other types of protein-specific immobilization including novobiocin-modified lipids to crystallize DNA gyrase,[42,43] ATP–lipid monolayers to immobilize ATP-binding proteins,[44] and dinitrophenyl(DNP)–lipid conjugates to crystallize anti-DNP IgG and IgE[45] (Figure 2). One drawback of this strategy, however, is the need to prepare unique affinity lipids for each new protein whose structure is sought. Unfortunately, the synthesis of these customized lipids can be very time consuming and difficult—or even impossible in cases where the proteins lack single, high affinity binding sites. This situation led investigators to search for a more general method to promote specific protein–lipid monolayer interactions for templating 2D crystallization.

Metal Affinity Ligand:Hexahistidine Interactions

In 1975, Porath and co-workers introduced the concept of immobilized metal affinity chromatography (IMAC)[46] for protein and nucleic acid separation. This method was refined by Hochuli et al.[47] who covalently grafted the classical metal chelating ligand, nitrilotriacetic acid (NTA), onto a chromatography resin via a modified lysine residue. NTA is a tetradentate ligand capable of occupying four positions in the coordination sphere of octahedral metals, leaving two positions available for interactions with proteins bearing appropriate ligands for metal coordination. Since the prosthetic group of histidine is imidazole, a ligand with high affinity for transition metals, proteins bearing surface histidines can be purified using IMAC resins bearing NTA ligands. Recombinant proteins that have been engineered to contain a repeating sequence of six (or more) histidines (i.e., generating a biosynthetic chelating ligand referred to as a "his-tag") can be readily purified by IMAC. Equilibrium constants of $K_d \approx 10^{-7}$ M[48–51] and 8×10^{-10}–10^{-13} M[52–54] have been reported for the his_6-protein:M^{2+} and NTA:Ni^{2+} binding interactions, respectively, enabling single-step purifications of the target protein in some cases. IDA- and NTA-based IMAC technology is now widely used with Cu^{2+} and Ni^{2+} (or Co^{2+}), respectively, to purify his-tag proteins for biochemical and structural characterization.

By merging the 2D crystallization and IMAC concepts, new opportunities for producing 2D crystals of many different histidine-tagged proteins are created that combine the advantages of specific his-tag:M^{2+}:NTA interactions with the self-assembly properties of lipids (Figure 1B). As in IMAC, small amounts of imidazole are believed to prevent nonspecific binding via surface histidines and favor specific interactions with the engineered his-tag, thus enabling the oriented immobilization of his-tag proteins that is needed to promote the 2D crystallization process. Binding of the his-tag protein to M^{2+}-charged NTA lipids is also reversible—either by competition with imidazole, complexation of the chelated metal ions with a stronger chelating agent such as EDTA, or by lowering the pH until the histidine residues are protonated (thus producing a weaker binding ligand for M^{2+} chelation). It is important to recognize that this method is not limited to proteins bearing the commonly used recombinant N-terminal his_6-tag. Naturally abundant surface histidines,[55] those put there by site-directed mutagenesis (see below), or his-tags installed after purification can be used as well. A major advantage afforded by introduction of histidine residues at specified locations on the protein surface is that it provides control over protein orientation at the interface. An additional benefit of this approach is that variation of the position of the histidines allows the visualization of multiple orientations of the protein, thus avoiding the "missing cone" problem encountered with 3D structures that are produced from tilt-series imaging of 2D crystals by TEM.

♦ *Synthesis of NTA– and IDA–Lipids*

NTA–Lipids

A list of the NTA lipids that have been developed for his-tag protein immobilization and crystallization applications appears in Table 3. The routes to these compounds share several common features, including the use of (1) glycerol- or dialkylamine-based lipid moieties, (2) carboxyl ester-protected NTA

Table 3. NTA lipids synthesized for protein immobilization & 2D crystallization applications

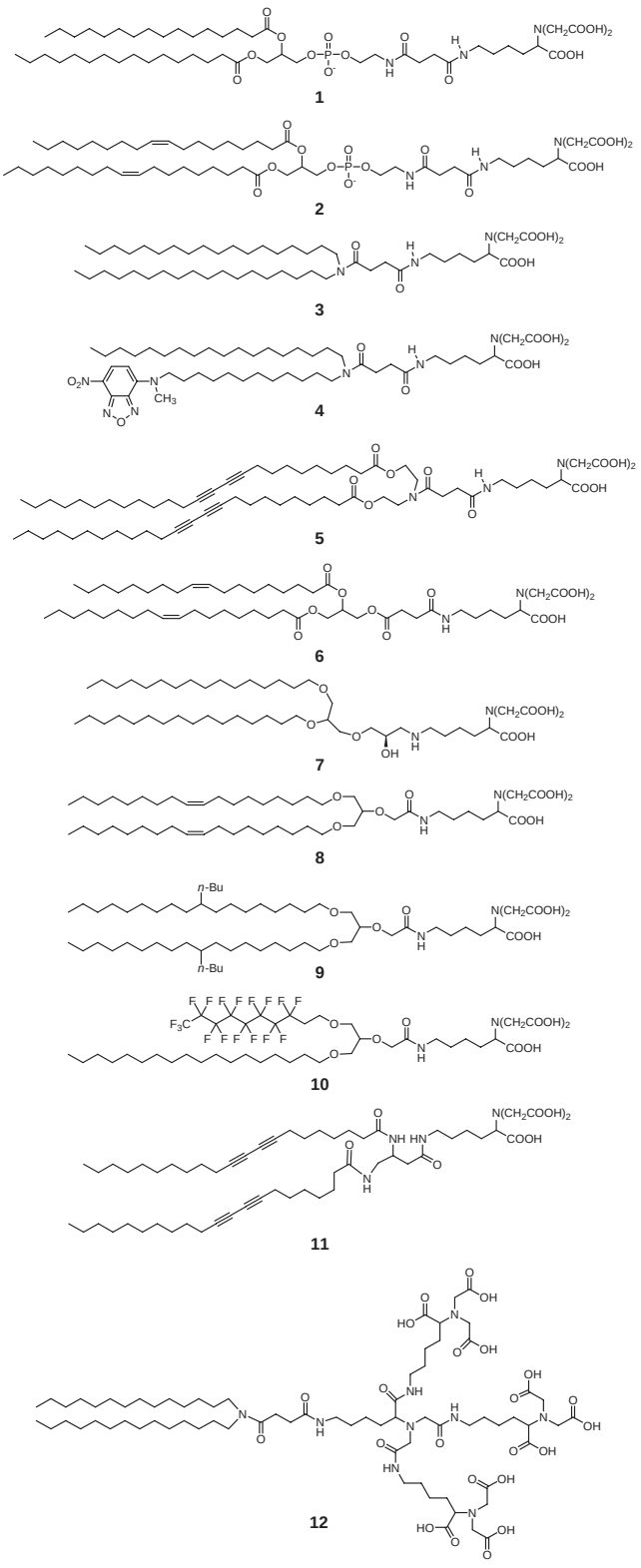

Continued on the next page.

Continued.

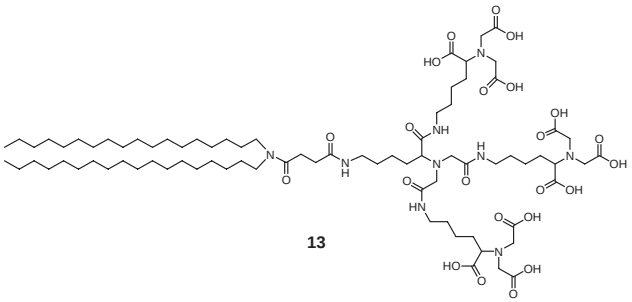

13

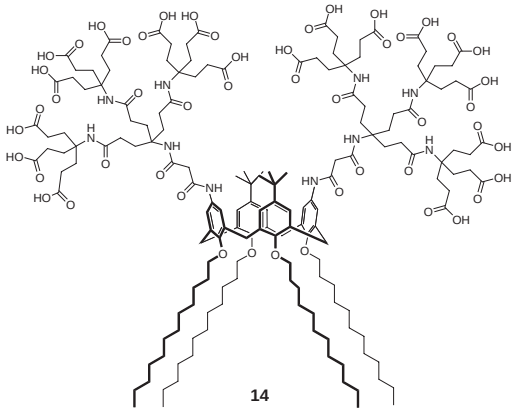

14

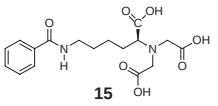

15

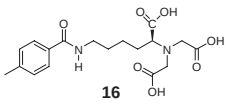

16

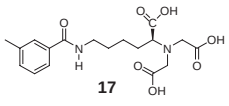

17

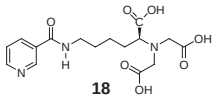

18

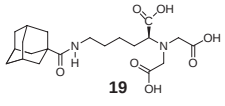

19

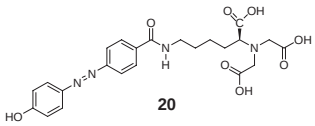

20

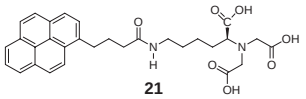

21

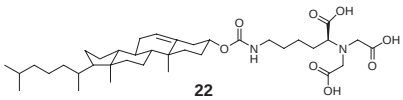

22

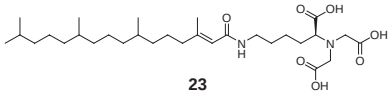

23

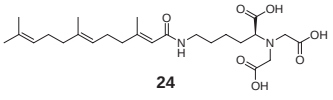

24

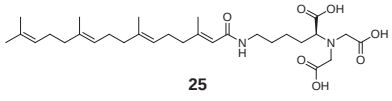

25

Continued on the right page.

Continued.

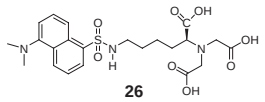

26

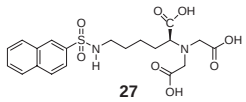

27

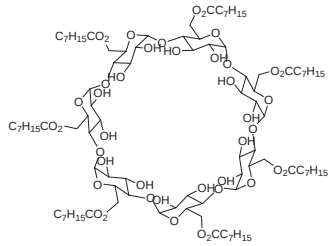

28

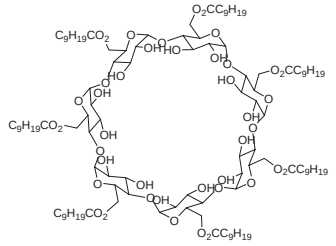

29

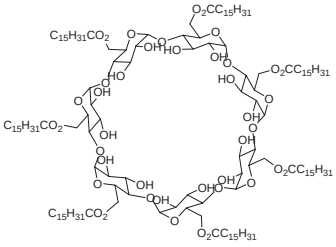

30

derivatives for enhancing their solubility in organic solvents to facilitate lipid coupling reactions, and (3) short bifunctional tethers to join the NTA and lipid substitutents.

Lipids **1**–**5** based on succinate as the tether group were prepared using the general synthesis scheme shown in Figure 3. Condensation of 1,2-dipalmitoyl-*sn*-glycero-3-phosphoethanolamine (**1**),[56] 1,2-dioleoyl-*sn*-glycero-3-phosphoethanolamine (**2**),[57] *N*,*N*-dioctadecylamine (**3**),[56] *N*-octadecyl-*N*-(12′-nitrobenzoxadiazole)dodecylamine (**4**),[58] *N*,*N*-di(2′-hydroxyethyl-hexatriconatate-10,12-diynyl)amine (**5**),[59] and 1,2-dioleoyl-*sn*-glycerol (**6**)[60] with succinic anhydride, followed by dicyclohexylcarbodiimide-mediated condensation of the intermediates with either unmodified lysine–NTA (**1** and **2**) or ester-protected forms of lysine–NTA (**3**–**5**) following deprotection gave the desired NTA lipids in modest yield.

Lipid **7** was produced by condensing unmodified lysine–NTA with 3-glycidyl-1,2-di-*O*-hexadecyl-*sn*-glycerol (Figure 4) in CTAB micelle solution.[61] Although this reaction was efficient, recovery of the desired NTA lipid was poor due to the difficulty in separating pure **7** from the CTAB dispersant.

Figure 5 shows the pathway developed for the synthesis of hydroxyacetyl-linked NTA lipids **8**–**10**. This method provided three fluidity-enhanced NTA lipids based on 1,3-di-*O*-oleylglycerol (**8**),[62] 1,3-di-*O*-(9′-butyl)octadecylglycerol (**9**),[63] and 1-*O*-(9′-butyl)octadecyl-3-*O*-perfluorooctylglycerol (**10**)[64] lyophobic groups.

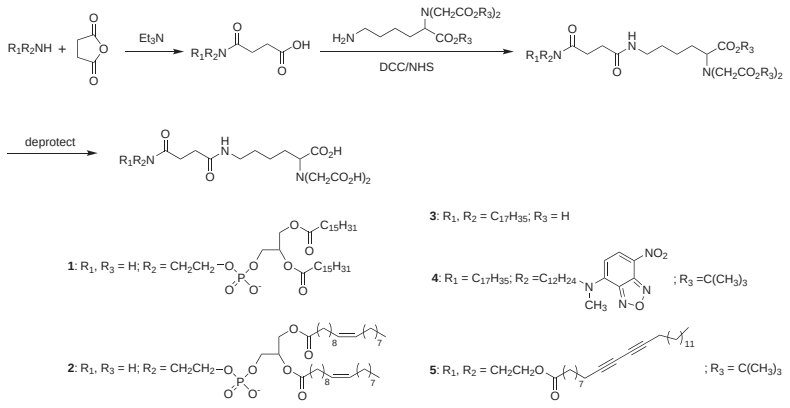

Figure 3. General synthesis pathway for succinamidyl-linked NTA lipids.

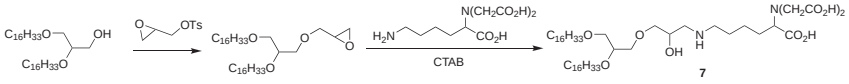

Figure 4. General synthesis pathway for glycidyl-linked NTA lipid.

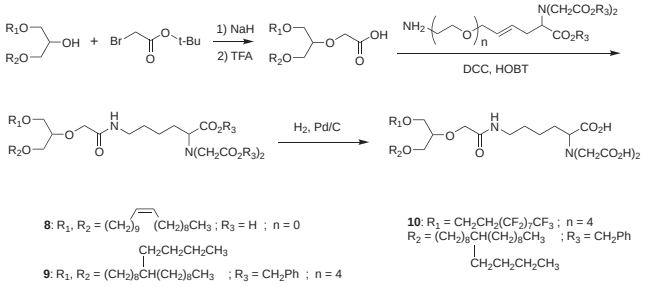

Figure 5. General synthesis pathway for carboxymethylamide-linked NTA lipids.

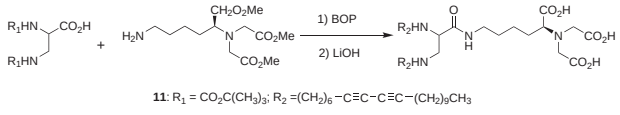

Figure 6. Synthesis of polymerizable amide-linked NTA lipid.

Lipid **11** was prepared by condensing lysine–NTA trimethyl ester with doubly Boc-protected 3-aminoleucine, followed by deprotection, acylation of the two amine substituents with a diacetylenic fatty acid, and saponification with lithium hydroxide in methanol (Figure 6).[65]

Lipids bearing multiple NTA ligands have also been prepared. Two tri-NTA compounds, **12**[66] and **13**,[67] differing by only the length of the hydrocarbon chains in the lipid anchoring substituents, have been prepared using the pathway shown in Figure 7. An unusual hexa-NTA derivative **14**,[68] prepared as shown in Figure 8 using a dodecyl ether-modified calix[4]arene scaffold, has also been reported. This material forms micelles instead of monolayers or lamellar structures in aqueous solution due to the size mismatch between the large hydrophilic headgroups relative to the short hydrophobic chains.

A family of non-covalent NTA lipids[69] has also been prepared by condensing various guest precursors bearing carboxylic acid, carboxylic acid chloride, or sulfonyl chloride substituents with the distal amino group of lysine–NTA trimethyl ester (Figure 9). Deprotection of these intermediates gave NTA guest ligands **15**–**27** in good to excellent yield. Complexation of these guests with β-cyclodextrin derivatives bearing decanoyl (**28**), dodecanoyl (**29**), or hexadecanoyl (**30**) modifications on the primary 6′-hydroxymethyl rim of the cyclodextrin (Figure 10) produces a host:guest complex at the air–water interface that is capable of immobilizing Ni^{2+}.

IDA–Lipids

Table 4 contains the list of IDA lipids that have been developed thus far. Like the NTA lipid syntheses, IDA synthesis pathways also have several features in common, including the use of (1) glycerol or 3-aminoleucine lipid backbones, (2) carboxyl ester-protected IDA derivatives to enhance their solubility in organic solvents during lipid-coupling reactions, and (3) short ethylene glycol tethers to link the IDA and lipid substitutents.

Lipids **31**–**33** were prepared by alkylating 1,2-dioctadecylglycerol (**31**),[70] 1,2-dioleylglycerol (**32**),[71] or 9-(1′-pyrenyl)-nonyl-2-octadecylglycerol (**33**)[72] with 1-methanesulfonyl-9-*O*-trityl-3,6,9-trioxanonane, followed by trityl replacement with diethyl iminodiacetate and saponification to give the desired products in modest yield (Figure 11).

Phospholipid derivatives **34**–**36** were produced using 2-bromoethyl-(**34** and **35**) or 2-hydroxyethyl-(**36**) phosphodiester precursors for installation of the IDA ligand substituent (Figure 12). These pathways differ only in that **34** and **35** undergo acylation with the corresponding acid anhydride in the final step of the reaction sequence, while **36** is prepared using an acylated phospholipid precursor that is condensed with iminodiacetic acid using an activated sulfonyl chloride intermediate.

Lipid **37** was prepared by reacting 1-*N*-Boc,10-diamino-4,7-dioxadecane with ethyl bromoacetate under basic conditions prior to condensing it with doubly Boc-protected 3-aminoleucine. Deprotection of the doubly Boc-protected intermediate, followed by acylation of the two amine substituents with a diacetylenic fatty acid, and saponification with lithium hydroxide in methanol/tetrahydrofuran gave the desired polymerizable

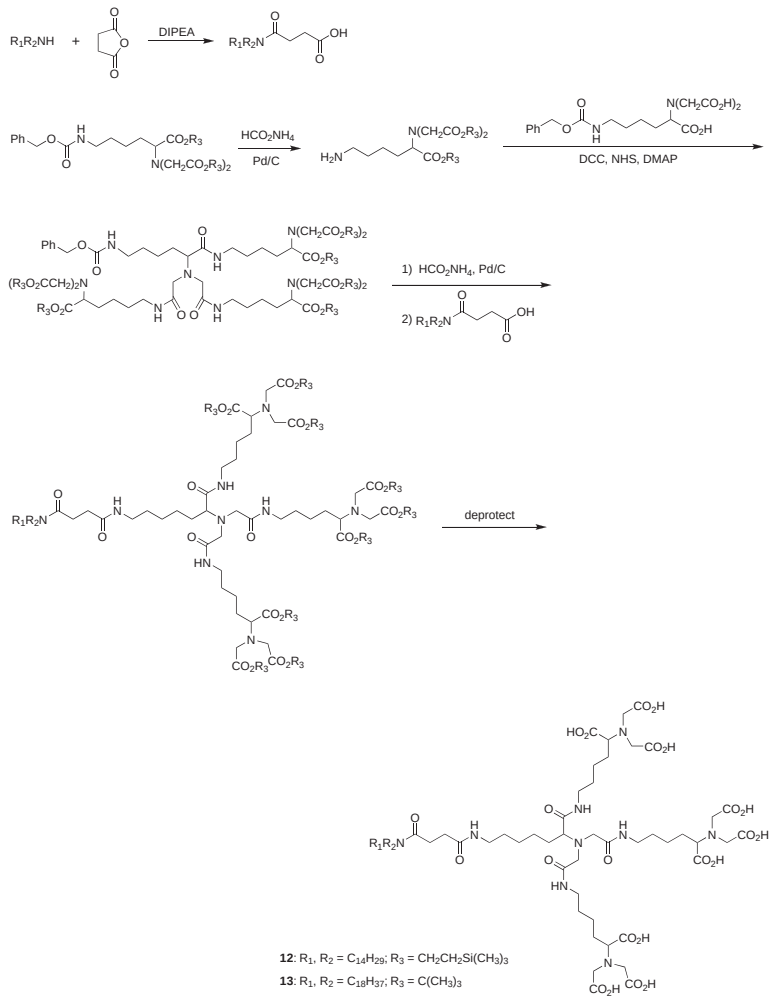

Figure 7. General synthesis pathway for succinamidyl-linked trisNTA lipids.

IDA lipid in good overall yield (Figure 13).[65]

The polymerizable sorbyl-modified phospholipid was prepared by condensing a Boc-protected triethylene glycol IDA precursor with 1-palmitoyl-2-[8-[(*E*,*E*)-2′,4′-hexadienoyloxy]octanoyl]-*sn*-glycero-3-phosphatidylethanolamine prior to TFA-mediated deprotection to give **38** in low overall yield (Figure 14).[73]

A family of dye-modified diacetylenic IDA derivatives have been prepared by condensing 10,12-docosadiynedioic acid in stepwise fashion with 1-[*N*,*N*-di(ethoxycarbonylmethyl)-amino]-10-amino-4,7-dioxadecane, and the corresponding amino dye derivatives, prior to deprotection to give **39**–**43** in modest to good yields (Figure 15).[74]

♦ *Protein Structure Elucidations Facilitated by Metal Chelating Lipids*

Background

Three different research groups reported the use of metal chelating lipids for immobilization of his-tag proteins in 1994. Their pioneering efforts are briefly summarized below.

Tampé and co-workers used the Langmuir film balance technique to monitor the complexation of metal ions to monolayers containing **1** or **3**.[56] Their results showed that the pressure-area isotherms of monolayers containing **1** or **3** were affected by the presence of Ni^{2+}. Since these NTA lipids bind Ni^{2+} and imidazole in a reversible manner, and can be stripped of the metal ion by addition of EDTA, they offer advantages over the biotin–streptavidin system that effectively lacks reversibility. Tampé et al. also showed that the binding process and emergence of surface patterns of his-tagged molecules were directly caused by his-tag protein:Ni^{2+}:NTA lipid complexation.[75]

Subsequent control experiments showed that proteins lacking a hexahistidine sequence did not bind to Ni^{2+}-activated monolayers of **3**[76] and that pairwise formation of his-tag molecules and Ni^{2+}:NTA lipid complexes occurs (demonstrated using fluorescence resonance energy transfer and fluorescence correlation spectroscopy).[58] Their experiments showed highly specific binding between NBD-labeled NTA lipids and rhodamine-labeled his-tag peptides. Tampé and co-workers later reported a more detailed investigation of his-tag protein immobilization kinetics using hexahistidine green fluorescent protein (his_6-GFP) and Ni^{2+}-activated NTA lipids via surface plasmon resonance (SPR) on 2:98 **3**:SOPC supported bilayers.[48] These studies showed that his_6–GFP binds rapidly under pseudo-first order conditions with an apparent second order association rate constant of $k_{assoc} = 2 \times 10^3\ M^{-1}\ s^{-1}$ and dissociates slowly ($k_{dissoc} = 2 \times 10^{-4}\ s^{-1}$) to yield a dissociation constant of

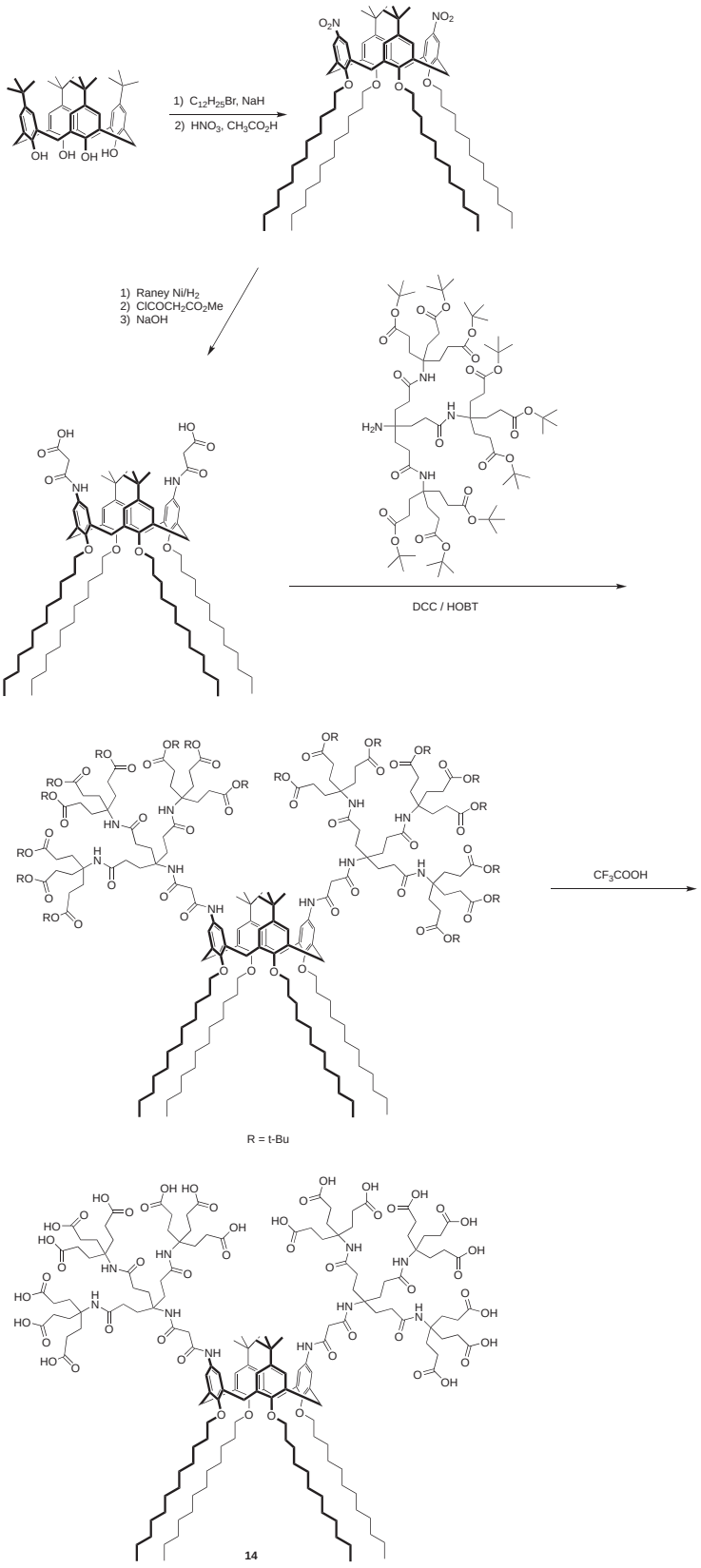

Figure 8. Synthesis pathway for calixarene-based hexaNTA surfactant.

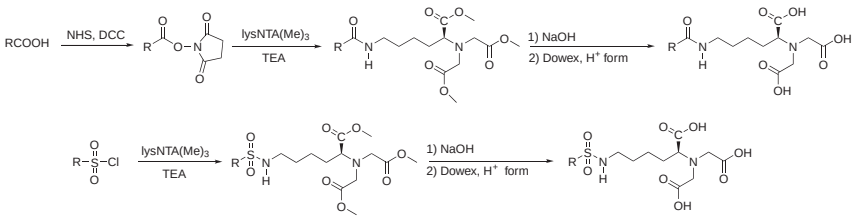

Figure 9. General synthesis pathway for carboxamide- and sulfonamide-linked NTA guest ligands.

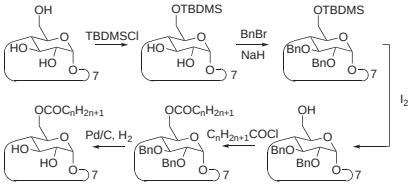

Figure 10. Synthesis pathway for 6-*O*-hepta(hexadecanoyl)-β-cyclodextrin (**30**).

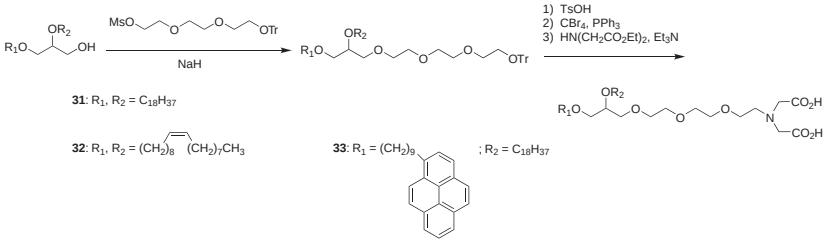

Figure 11. General synthesis pathway for triethyleneglycol-linked IDA lipids.

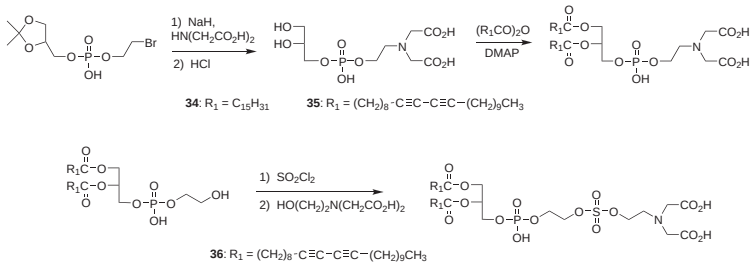

Figure 12. Synthesis pathways for IDA-modified phospholipids.

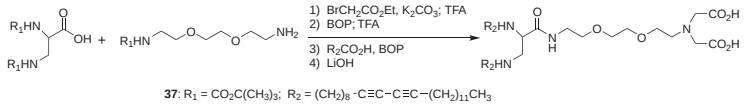

Figure 13. Synthesis pathway for polymerizable diethyleneglycol-linked IDA lipid.

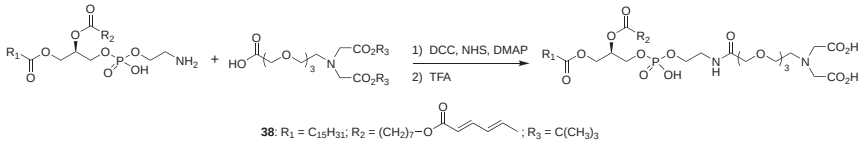

Figure 14. Synthesis pathway for sorbyl-modified IDA lipid.

Table 4. IDA lipids synthesized for protein immobilization & 2D crystallization applications

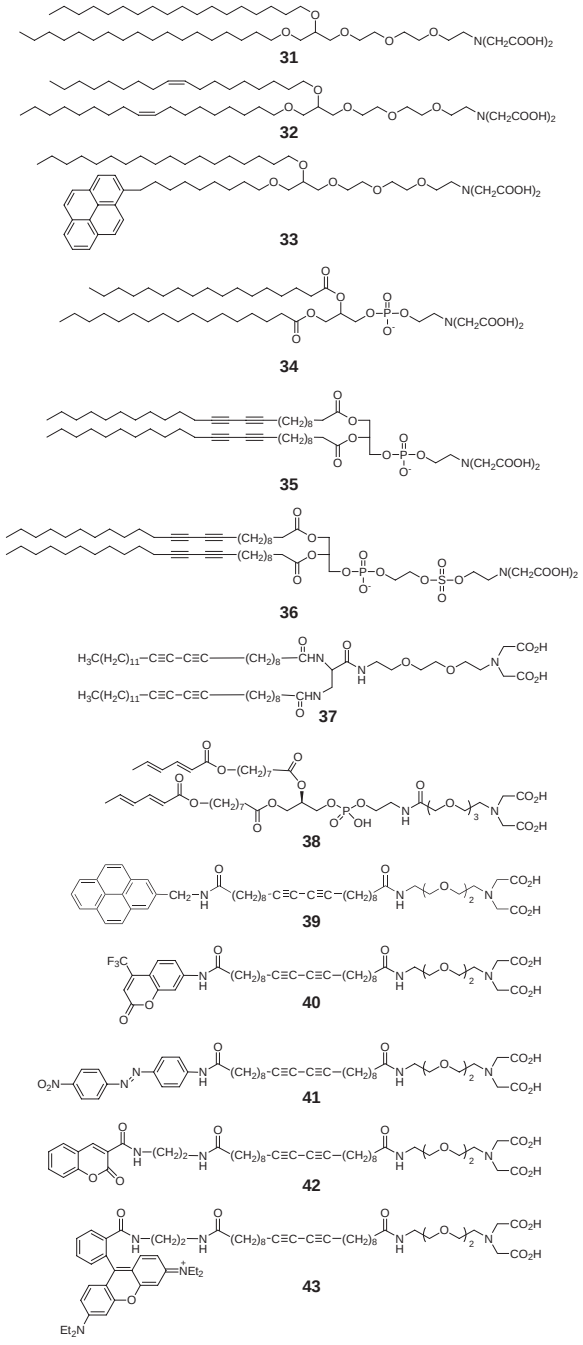

$K_{dissoc} = 1.1 \times 10^{-7}$ M. Less than 2% non-specific adsorption was observed in these experiments. Fluorescence microscopy of supported monolayers, prepared by Langmuir–Schaeffer transfer of his–GFP–Ni^{2+}–**3** monolayers onto octadecatrichlorosilyl-treated glass, revealed the presence of micron-sized weakly fluorescent domains that were attributed to 2D aggregates of his_6–GFP.[48]

Kubalek, Le Grice, and Brown reported the use of Ni^{2+}:**2** for immobilization of his-tag HIV-1 reverse transcriptase (HIV-RT).[57] Their work showed that 2D crystals of HIV-RT were formed under Ni^{2+}:**2** monolayers within minutes upon exposure to dilute HIV-RT solutions. The 2D crystals formed were stable in the presence of negative stain and diffracted strongly to ca. 21 Å resolution. Control experiments showed that his-tag HIV-RT did not bind to films lacking **2**.

Finally, Arnold and co-workers used Langmuir monolayers in 1994 to promote the binding of myoglobin, a histidine-rich protein, via Cu^{2+}:IDA lipid complexation.[70] Pressure-area isotherm data showed that the presence of Cu^{2+} at the air–water interface was responsible for enhancing the rate and extent of myoglobin binding on the Cu^{2+}:IDA lipid monolayer film. Subsequent efforts focused on the 2D crystallization of streptavidin mutants using Cu^{2+}:IDA complexes.[55,71] Fluorescence microscopy studies revealed that the binding and crystallization of streptavidin is promoted by the simultaneous coordination of two surface-accessible histidine residues by the Cu^{2+}:IDA lipid.[71] Control experiments with cytochrome b_5, which lacks surface-accessible histidines or a his-tag, did not produce a protein adsorbate at the Cu^{2+}:IDA lipid interface, thus supporting their conclusion of histidine-specific adsorption.[72]

Determination of Protein Structures Using Metal Chelating Lipid Interfaces

Further development of interfacial protein crystallization has generally occurred along two lines of investigation. The first involves the creation of new tools for protein crystallization, such as (1) automated methods for analyzing flash-vitrified protein samples using cryogenic transmission electron microscopy (cryo-TEM),[77] (2) adaptation of lipid rod phases as matrices for helical crystallization and reconstruction of protein structures (see below), (3) prediction of protein crystallization conditions using relative crystallizability,[24] surface volume and diffusion kinetics[23] parameters, or (4) investigation of factors affecting crystal growth[78–82] and epitaxy.[40] The second line of investigations has used the existing lipid templating tools for nucleating and growing 2D protein crystals for structure elucidation. These efforts have led to medium resolution structures (i.e., 3–39 Å) for several different proteins using specific lipid–protein interactions that were not of the hexahistidine–metal ion complexation type (Table 5). Protein structural elucidations that have employed polyhistidine:metal ion:metal chelating lipid complexes as a key step in the production of 2D crystals for analysis are briefly summarized below.

Streptavidin. To date, there are relatively few systematic studies that focus on how the properties of the lipid interface and bulk solution affect the size, morphology, and quality of 2D protein crystals that are grown from a lipid-templating interface. The best-known case is streptavidin, which has been shown to display pH-,[80] ionic strength,[82] and amino acid residue-dependent[80,81] crystallization behavior on biotinylated lipid monolayers. Intriguingly, one study comparing streptavidin crystals grown on biotinylated lipid monolayers with those grown on Cu^{2+}:**32** monolayers found that the crystal morphs were similar by negative-stain transmission electron microscopy (Figure 16), even though their binding modes and gross morphologies were different.[55,95] Vogel and co-workers further showed using Brewster angle and light-scattering microscopy that streptavidin crystal formation is sensitive to the applied surface pressure at the air–water interface such that the 2D streptavidin crystals dissolve if the monolayer is expanded or compressed.[96,97] These results strongly suggest that the

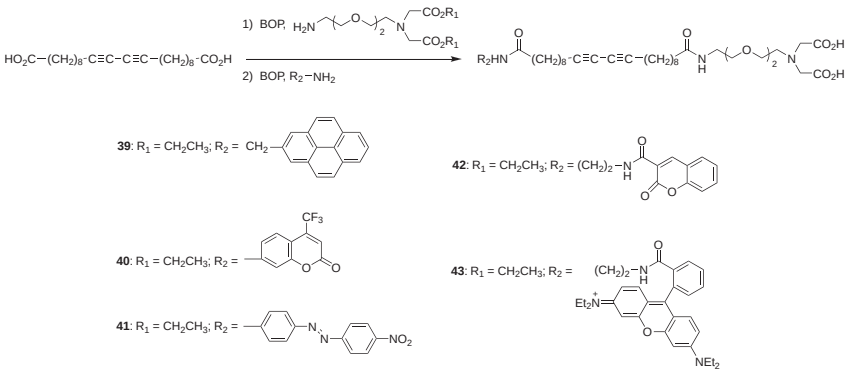

Figure 15. General synthesis pathway for polymerizable IDA lipids with fluorophore modifications.

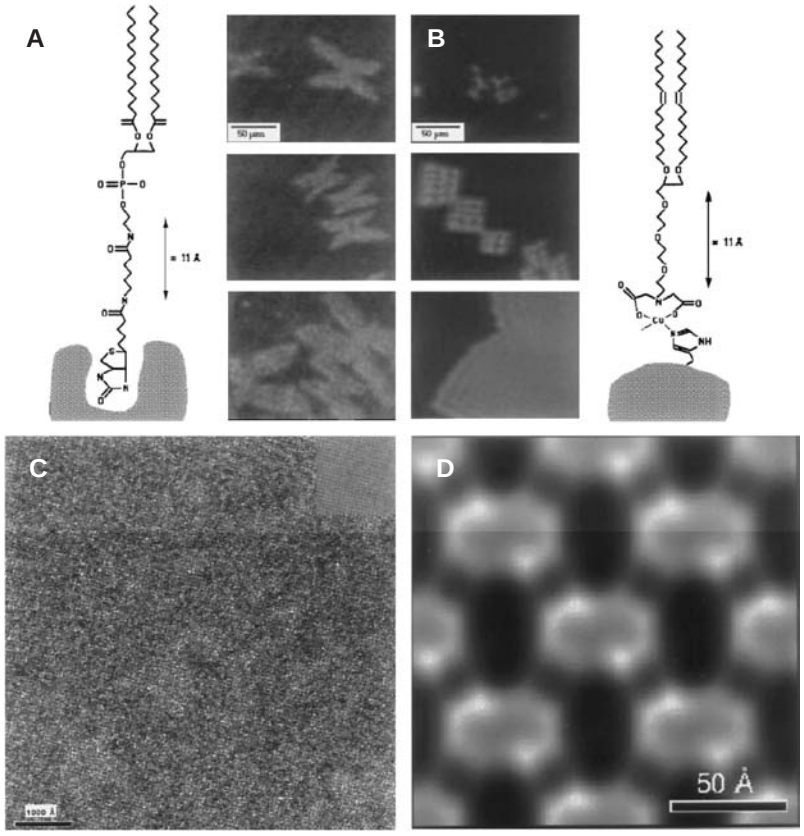

Figure 16. Appearance of streptavidin 2D crystals grown on biotin-DPPE (A) and Cu^{2+}:**32** (B) lipid monolayers by Brewster angle microscopy. Negative stain transmission electron microscopy (C) and image reconstruction produces the streptavidin projection map shown in (D) at 15 Å resolution. Reproduced with permission from *Biophys. J.* **1998**, *74*, 2674.

protein–lipid binding strength and interfacial dynamics play a significant role in establishing different protein–protein contacts beneath the lipid template and in promoting epitaxial growth of the protein into 3D crystals.[40,98]

His-tag Green Fluorescent Protein. Reversible adsorption of his_6-GFP on Ni^{2+}-activated DMPC:**3** monolayers supported on silanized glass was first reported by Tampé and co-workers.[48] Adsorption occurs predominantly in the condensed regions of the monolayer that are enriched in **3** and exclude the fluorescently labeled lipid TR–DPPE (Figure 17A). Loss of GFP fluorescence upon addition of EDTA confirms that Ni^{2+} ligation by **3** is required for his_6–GFP binding. Recent AFM experiments by Galla and co-workers[51,99] have shown that his_6–GFP domain formation occurs when nanomolar concentrations of the protein are exposed to mica-supported bilayers of 4:1 DPPC:**6** in the presence of Zn^{2+}. Since GFP is a β-barrel structure that is approximately 4.2 nm high and 2.4 nm in diameter, the step heights in the line scan shown in Figure 17B suggest that his_6–GFP monolayer domains ranging between 50–150 nm in diameter are formed such that the proteins are oriented with their major axes perpendicular to the mica surface.

His-tag Capsid Proteins. Thompson and co-workers first synthesized NTA lipid **7**, demonstrated its ability to chelate Ni^{2+} by atomic absorption spectroscopy, and showed that it

Table 5. Protein structures determined by analysis of 2D protein crystals grown on lipid interfaces using specific ligand–protein interactions

Protein	Lipid Template (mol:mol)	Analysis Method	Resolution	Ref.
Yeast RNA polymerase II	1:3.2 Octadecyl amine:EPC	electron crystallography, tilt series	16 Å	33
Streptavidin	1:4 Biotin–DPPE: DOPC	electron crystallography	3 Å	41
DNA gyrase B	Novobiocin–phospholipid	electron crystallography, tilt series	25–30 Å	43
Bacterial S-layer	DPPC; DPPE	negative-stain TEM + FT analysis; X-ray reflectivity	<30 Å	83–87
Sticholysin II	EPC	electron crystallography, tilt series	15 Å	88
Annexin V	20–95% DOPS:Ca^{2+} in DOPC	cryo-TEM + FT analysis; AFM	20 Å	89; 90
Rabbit C-reactive protein	5:1 EPC:lysoPC + Ca^{2+}	negative-stain TEM + FT analysis	22 Å	91
Shiga toxin B subunit	4:6 erythrocyte Gb3:DOPC	cryoTEM + FT analysis	8.5 Å	92
M. tuberculosis heat shock protein	1:5 Octadecyl amine:DOPC	negative-stain TEM + FT analysis	22 Å	93
Herpes simplex DNA binding protein ICP8	7:3 DLPC:DDAB	negative-stain TEM + FT analysis	39 Å	94

could be used to facilitate the 2D crystallization of his-tag Moloney murine leukemia virus capsids (his_6-MoCA) at the air–water interface.[61] Negative-stain TEM data showed that his_6-MoCA crystallized over the entire surface of the lipid monolayer with few protein-free zones. Cryo-TEM was used to determine the his_6–MoCA structure at 9.5 Å resolution. A 2D projection map derived from the cryo-TEM data showed a cage-like network with hexamer rings that were surrounded by hexagonal and triangular protein-free cage holes that were proposed as docking sites for the matrix and nucleocapsid components of the virus. AFM studies of his_6–MoCA on mica-supported 9:1 EPC:**7** supported bilayers revealed a cage network of symmetrical hexamers,[100] whereas negatively stained crystals prepared on bilayer vesicles and imaged by TEM revealed structures comparable to those obtained on fluid monolayers.[101] Based on their examination of his_6–MoCA 2D crystals that had been grown on monolayers of **6**, Yeager et al.[102] proposed a unifying model of how different viral morphologies can emerge by incorporation of penton "defect" sites at various points in the hexagonal lattice to produce an enclosed structure.

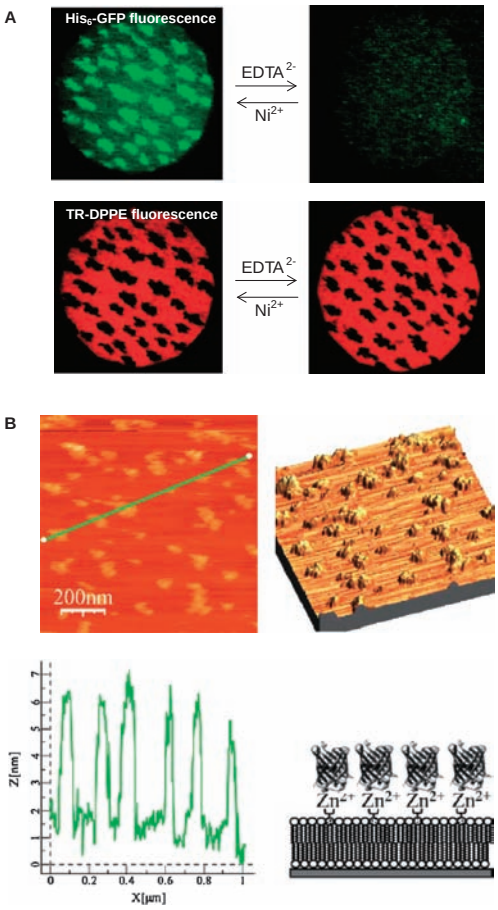

Figure 17. Reversible adsorption of his_6-GFP on Ni^{2+}-activated DMPC:**3** monolayers supported on silanized glass (A).[48] GFP adsorption occurs predominantly in the condensed regions of the monolayer that are enriched in **3** and exclude the fluorescently labeled lipid TR-DPPE. The TR-DPPE-rich domains are unaffected by the addition of EDTA, however, GFP fluorescence is lost upon addition of EDTA showing that his_6-GFP binding requires the presence of Ni^{2+}. His_6-GFP crystallization occurs on mica-supported bilayers comprised of Zn^{2+}-activated DPPC:**6** (B). His_6-GFP domains 50–150 nm in diameter and ca. 4 nm high are observed. Data in (A) reproduced with permission from *Biol. Chem.* **1998**, *379*, 1151. Data in (B) reproduced with permission from *Biochem. Biophys. Res. Commun.* **2005**, *327*, 174, and *Biochem. Biophys. Res. Commun.* **2005**, *326*, 298.

His-tag human immunodeficiency virus 1 capsid (his_6-HIV-1 CA) has also been crystallized on 9:1 EPC:**7** monolayers and analyzed by cryo-TEM.[25] Analysis of the EM images at 24 Å resolution revealed that membrane-bound his_6-HIV-1 CA proteins organize into a cage-like network consisting of hexamers and trimers that surround protein-free holes (Figure 18). Dock-

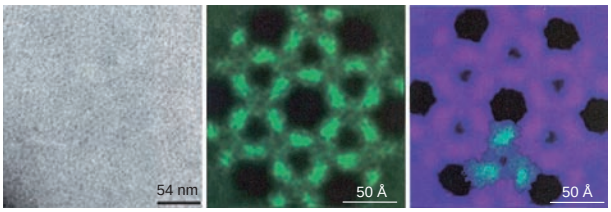

Figure 18. HIV-1 CA arrays crystallized on Ni^{2+}-activated 9:1 EPC:**7** monolayers at the air–water interface. Left: Cryo-TEM image of HIV-1 CA arrays. Center: 2D projection map of HIV-1 CA arrays at 2.4 nm resolution (determined by image analysis of data at left). Right: Overlay of matrix trimer structure onto HIV-1 CA array. Reproduced with permission from *J. Biol. Chem.* **1998**, *273*, 7177.

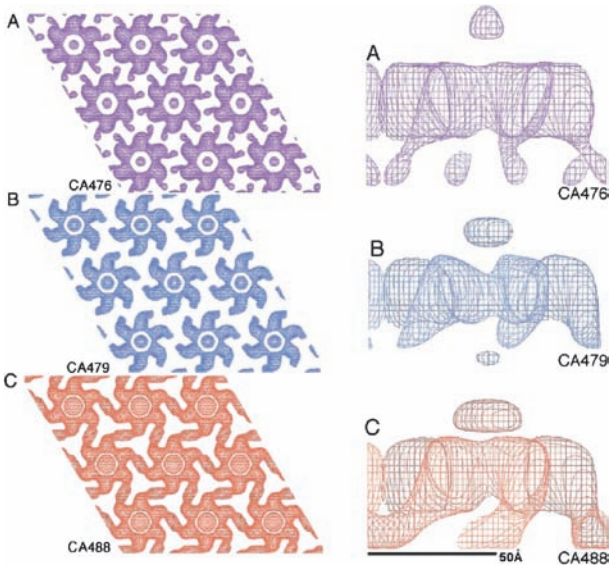

Figure 19. Rous sarcoma virus capsid structures for CA476 (A), CA479 (B), and CA488 (C) normal (left) and parallel (right) to the membrane, with the capsid-membrane contact depicted at the center of the hexamers (left) and at the top of the capsid profile (right). Reproduced with permission from *J. Mol. Biol.* **2002**, *316*, 667.

ing of the HIV-1 matrix protein trimer from the Brookhaven Protein Data Bank for comparison with HIV-1 CA showed that the matrix residues previously known to interact with the HIV-1 gp120/gp41 envelope protein complex were oriented toward the cage holes. The complementarity of these structures suggests that (1) the observed his_6-HIV-1 CA structure is likely to be that found in intact virus particles and (2) assembly of the capsid lattice, which is promoted by binding to membrane surfaces, likely serves as a necessary first step that enables it to scaffold the subsequent assembly of other virion components to produce infectious particles within host cells.

Two-dimensional crystals of Rous sarcoma virus capsids in three different forms (CA476, CA479, and A488) after proteolytic processing have been formed using lipid monolayers containing Ni^{2+}-charged **6**.[103] These 2D crystals were analyzed by tilt-series cryo-TEM and image analysis (Figure 19). Differences in the structures formed by these variants suggest that the N-terminal domains are in contact with the membrane interface

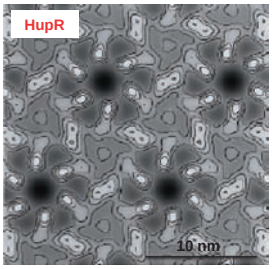

Figure 20. Structure of HupR determined by image analysis of 2D crystals formed on mixed monolayers of **8** and DOPC or DOPE. Reproduced with permission from *J. Mol. Biol.* **1997**, *274*, 687.

and share a similar hexameric ring motif, while the C-terminal domains are more structurally diverse and form the interconnects between the hexameric rings.

His-tag HupR.[62] The transcriptional regulator from the photosynthetic bacterium *Rhodobacter capsulatus* was crystallized in 2D using Ni^{2+}-activated monolayers of **8** in various molar ratios with DOPE or DOPC. The protein, characterized by negative-stain TEM image analysis at 18-Å resolution, folds into an L-shaped motif that then assembles into a hexameric propeller-like structure (Figure 20).

His-tag AcrA.[104] The *Escherichia coli* multidrug efflux complex AcrAB–TolC confers drug resistance to this organism by pumping antibiotics out of the cell in a proton motive force-dependent manner. Ni^{2+}-activated monolayers of 1:1 DOPG:**6** were used to generate 2D crystals of C-terminal His_6-AcrA for structural determination via electron crystallography of negatively stained samples. The 20-Å resolution structure consists of ring-like objects with a central diameter of 30 Å (Figure 21). The dimensions of the structure were consistent with the length of monomeric AcrA in solution determined by light scattering and hydrodynamic measurements.

His-tag Rhinovirus 2.[105] Dynamic force microscopy has been used to study the attachment of human rhinovirus 2 (HRV2) particles to POPC:**6** lipid bilayers supported on mica. Recombinant very-low density lipoprotein receptor fragment, fused at the N-terminus to maltose binding protein (MBP) and containing a hexahistidine-tag at its C-terminus (MBP-VLDLR1-8-His_6), produced dense quasi-crystalline monolayers of HRV2 particles of 30 nm diameter when the NTA lipid was charged with Ni^{2+} (Figure 22).

His-tag Proteosome.[106] Electron microscopy and atomic force microscopy has been used to investigate recombinant 20S proteosomes bearing his-tags in different positions on the protein on Ni^{2+}-activated 1:9 **3**:SOPC lipid bilayers. TEM images showed that proteasomes bearing his-tags at their sides displayed exclusively side-on views, while proteasomes bearing his-tags at their ends displayed exclusively end-on views and tended to crystallize in two dimensions when oriented vertically in this manner (Figure 23). This is the first clear evidence that the ability of a his-tag protein to crystallize can be affected by the placement of the his-tag. It was also found that the proteolytic activity of proteasomes was retained even after they had been immobilized on the chelating lipid interfaces.

His-tag Myelin Basic Protein.[107] Planar arrays of myelin basic protein (native and deiminated) have been generated on Ni^{2+}-activated lipid monolayers of **6** and either liver phosphoi-

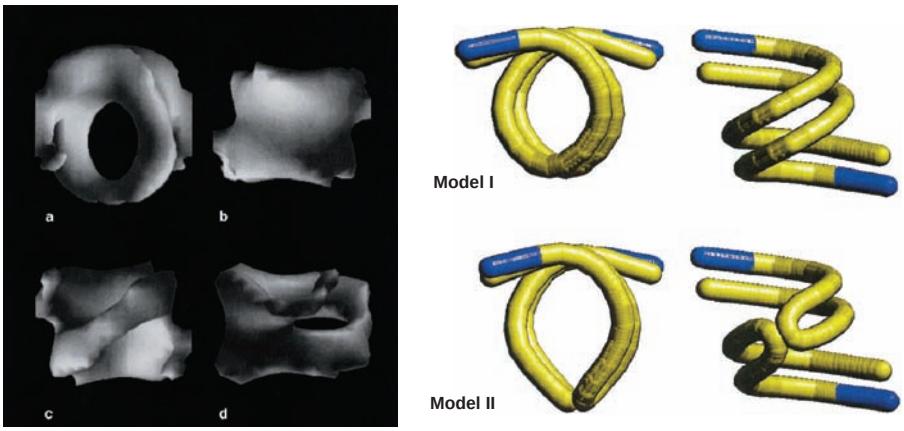

Figure 21. AcrA structure determined by electron crystallography of 2D crystals grown on 1:1 DOPG:**6** monolayers. Views b–d are from the top, left and bottom sides of the circular structure shown in a. Models I and II are proposed to account for the AcrA structure shown in a–d. Reproduced with permission from *J. Struct. Biol.* **2001**, *136*, 81.

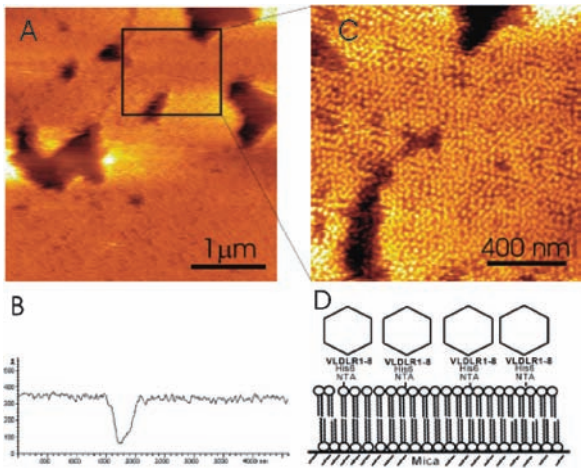

Figure 22. Human rhinovirus 2 bound to Ni^{2+}-charged 95:5 POPC:**6** monolayers. (A) Low-resolution AFM image of a densely packed HRV2-monolayer. (B) Line scan across array and defect site showing the 30 nm diameter of the virus. (C) High-resolution AFM image of the area shown in (A). (D) Schematic showing the specific interaction between human rhinovirus 2 and MBP-VLDLR1-8-His_6 used to immobilize the virus on the supported membrane. Reproduced with permission from *Single Mol.* **2001**, *2*, 99.

nositol or brain phosphatidylinositol-4-phosphate. When the osmolyte tetramethylamine-*N*-oxide was added, the crystallinity of the arrays increased and induced epitaxial growth of protein arrays, particularly in the case of the mutant protein. Unfortunately, none of the assemblies was sufficiently ordered to produce high-resolution structures.

Protein Immobilization Using Multi-NTA Lipids

Lipids bearing multiple NTA ligands have been synthesized for immobilization of targeting ligands for liposomes[66,67,108–110] or developing stable micelles for drug delivery and vaccine applications.[68] Constructs bearing multiple NTA ligands with stronger ligand:Ni^{2+}:his-tag interactions have also been prepared for protein immobilization on solid surfaces[111] or fluorescent labeling of his-tag proteins.[112]

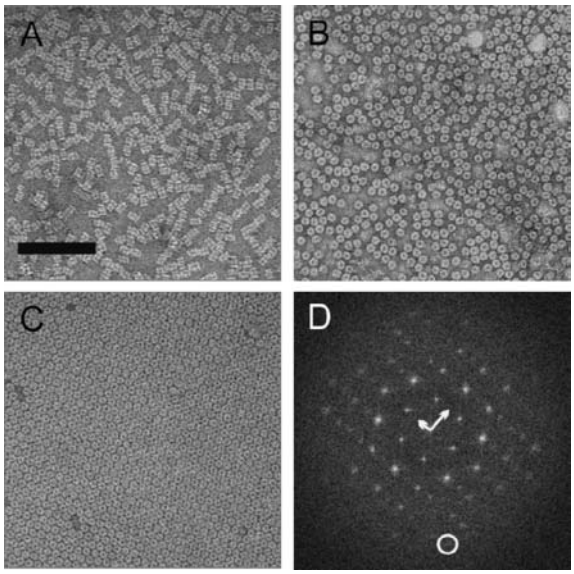

Figure 23. Effect of his-tag placement on 20S proteosome immobilization on 1:9 **3**:SOPC bilayers after charging with Ni^{2+}. (A) C-terminal His_6 proteasomes tagged on their sides show exclusively side-on views. (B) Proteasomes tagged at their end loops uniformly display end-on views. (C) N-terminal His_6 proteasomes form large 2D arrays. (D) Power spectrum calculated from the two-dimensional crystal in C. Scale bar in A–C: 100 nm. Reproduced with permission from *J. Biol. Chem.* **2002**, *277*, 36321.

Protein Crystallization on Lipid Rod Templates

Determination of a high-resolution 3D protein structure using electron diffraction requires the collection of a time-consuming tilt series of TEM images followed by reconstruction analysis. Since there are limits to the range that the transmission electron microscope stage can be tilted, and the sample is often degraded during a tilt series by sequential exposure of the 2D crystal to the electron beam, this method often leads to structures of modest resolution (ca. 15 Å). Wilson-Kubalek and co-workers[60] have developed a technique to overcome these difficulties by using liquid-phase galactosylceramide lipid tubule templates

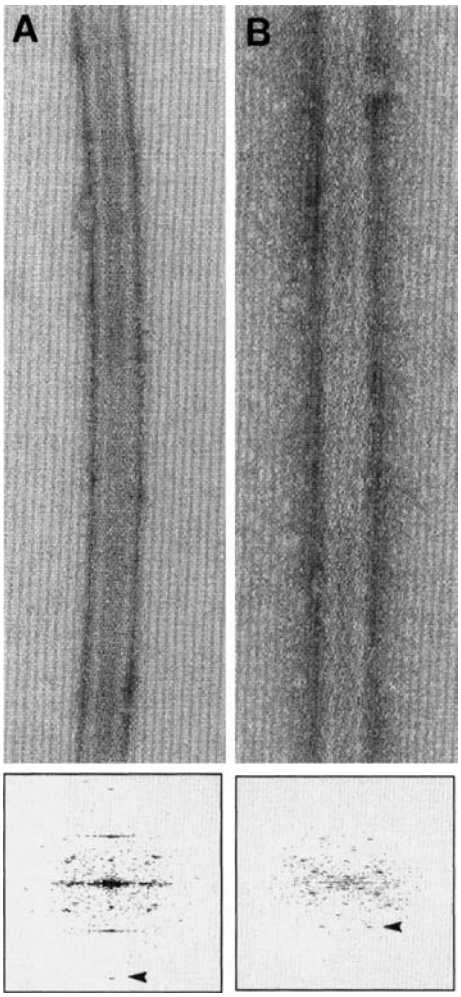

Figure 24. Helical arrays of his-tag Fab 3B3 (A) and FabAP7 (B) grown on GalCer lipid tubules containing 10 mol % **6**. TEM images (1% $UO_2(OAc)_2$ staining) are shown at the top (magnification × 140,000) and diffraction patterns calculated by helical reconstruction of the TEM data are shown at the bottom (arrowhead depicts visible diffraction peak at $1/30\,Å^{-1}$). Reproduced with permission from *Proc. Natl. Acad. Sci. U.S.A.* **1998**, *95*, 8040.

with diameters of approximately 270 Å that have been doped with low molar ratios of NTA chelating lipids or charged lipids to promote specific interactions with the lipid template surface (Figure 24). These lipid tubules enable 2D crystallization of his-tag proteins such that one TEM image could be used to reveal all orientations of the adsorbed molecules, thus eliminating the need for a tilt series or multiple his-tagging of the protein. In this manner, 3D structures could be rapidly calculated using semi-automated helical analysis.[77] The primary focus of this 1D lipid template has been the elucidation of new protein structures such as perfringolysin O,[113–115] however, one study has focused on developing a deeper understanding of the underlying principles involved in helical protein crystallization using the well-known streptavidin:biotin–lipid system.[116] Single-wall carbon nanotubes with an adsorbed lipid layer have also been proposed as 1D templates for helical crystallization of proteins,[117] although no applications of this system have appeared thus far.

High-resolution structure determination by electron microscopy is developing in two other areas. Combined crystallographic, molecular modeling and single particle analysis (electron tomography)[118] has been used to overcome resolution limitations arising from conformational variation of the protein, disorder in the 2D crystal lattice, or specimen defects such as deviation from flatness. This is a low-to-medium resolution approach that is best suited for multi-protein complexes or other large, complex structures that are not amenable to crystallization. Crystallization on lipid layers is also undergoing improvements in the areas of sample transfer,[119,120] development of detergent-resistant monolayers for 2D crystallization of integral membrane proteins,[121] utilization of supported bilayer membranes for crystallization of Annexin V,[122] and the design of novel lipids with novobiocin[123] or dichlorophenylurea[124] headgroups to promote specific protein–lipid interactions at the monolayer interface. These strategies seek to promote the formation of well-ordered 2D crystal arrays to serve as seeds for 3D crystal growth so that they can be analyzed at high-resolution X-ray diffraction. Efforts focused on improving the crystal growth process are described below.

♦ Approaches for Controlling Protein Crystal Nucleation and Growth

Current approaches to the rational control of protein crystallization have utilized different strategies, including relative crystallizability, criteria based on surface and volume diffusion kinetics, microfluidic systems that utilize nanoliter volumes of protein solution, and nanostructured interfaces whose properties can be tailored to the protein under investigation. The merits of the latter two approaches are briefly described below.

Crystal Growth Control Using Microfluidics

Slow concentration of protein solutions within microfluidic chambers bearing sessile droplets that are connected to empty microfluidic chambers for controlled evaporation has been described by Kenis and co-workers.[15,125] This approach provides precise control over the extent and rate of protein supersaturation by varying the dimensions of the protein and evaporation chambers in a multi-well format. Microfluidic arrays of these evaporation chambers have been used to discover the conditions that induce the formation of well-ordered crystals of lysozyme,[15] thaumatin,[15] and γ-glycine.[125]

Ismagilov and co-workers have used a different strategy for producing supersaturated protein solutions within microfluidic channels.[12–14,126–128] Their crystallization systems are based on convergent flow designs that bring together the protein solution, a precipitant, buffer, and a carrier fluid that enables the isolation of discrete droplets of protein/precipitant mixture within a carrier fluid stream. The droplets are then transported through serpentine microfluidic channels to promote fluid mixing that initiates nucleation and protein crystal growth once the flow is stopped and the system incubated. Crystals exceeding 50 μm in length have been grown in this manner from solutions of thaumatin, bovine liver catalase, and glucose isomerase.[12] The process typically involves the formation of protein precipitates or microcrystalline showers upon rapid mixing, followed by slow dissolution of the initially produced protein phase and nucleation of more ordered crystal growth. The number and size

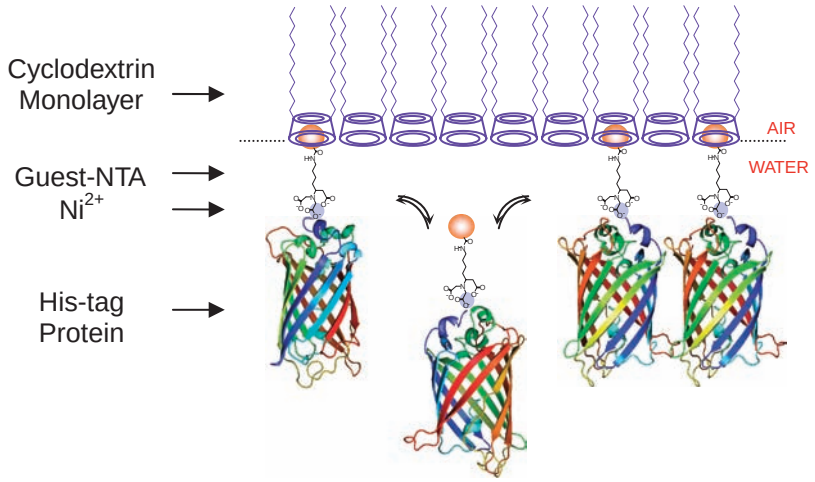

Figure 25. Site-hopping concept for 2D crystallization of proteins using cyclodextrin:NTA–ligand:Ni^{2+} complexation. Crystal formation and long-range order are influenced by host–guest interactions, site–site hopping rates, lateral diffusion rates of the protein–guest–host complex, and relative strength of protein–protein vs. host–guest interactions.

of crystals grown is strongly influenced by the dimensions of the microfluidic channels and the flow velocity employed, such that the nucleation rate is governed by the area and lifetime of the interface between the protein and the precipitant solutions.[126] Crystal growth from solutions whose concentrations are just below those required for crystallization have also been achieved by slow removal of water from the sample by allowing water diffusion through the PDMS channel walls (e.g., by maintaining the PDMS device in a dry environment) or into the carrier fluid (e.g., by choosing a carrier with low water solubility) to achieve the necessary level of supersaturation for promoting crystallization. A distinct advantage provided by the microfluidic approach is the ability to directly load the protein crystals grown within the microfluidic channels into X-ray capillaries for diffraction analysis.[13]

Crystal Growth Control by Varying Nucleation Density and Interfacial Dynamics

Recent developments in the field of dip pen nanolithography (DPN) and interfacial design offer new approaches for controlling the nucleation and growth of protein crystals. Mirkin and co-workers have demonstrated the controlled growth of polypeptide single crystals using DPN.[129] Deposition of poly-DL-lysine hydrobromide as a DPN ink promoted its crystallization as large, thin triangular crystals in pseudo-epitaxial registry with the mica substrate at 25 °C. Crystal growth was strongly influenced by the sample humidity, whereas scan direction and speed had little or no effect. The crystal edges appeared to grow more rapidly than the crystal thickness due to strong electrostatic interactions between poly-DL-lysine and the negatively charged mica substrate. The crystal morphology was also affected by the temperature of the DPN-mediated crystallization process, with cubic crystals forming at 35 °C. This work suggests that protein crystal growth may be controllable by utilizing highly periodic substrates as nucleation templates and localized flow to the template as a means to control crystal growth rates.

Access to such highly periodic interfaces is not limited to inorganic materials such as mica or single crystal silicon and gold. Ravoo and Darcy reported two amphiphilic cyclodextrins as a novel type of liposome-forming surfactant that forms nanostructured interfaces.[130] Two years later, Reinhoudt and co-workers introduced the concept of "molecular printboards" based on amphiphilic thioether cyclodextrins.[131] Molecular printboards are monolayer films of amphiphilic host molecules deposited on solid substrates that can accommodate guest molecules of varying binding strength. The guest molecules can be deposited onto the host monolayer film with positional control using techniques such as DPN.[132,133] The binding strengths and dynamics of guest ligands on the host substrate can be manipulated as well using a variety of techniques. The most commonly used host molecules are cyclodextrins (CD)[131–138] and calixarenes,[139–141] both of which can be immobilized on gold, silicon wafers, and glass substrates. Size-complementary hydrophobic interactions between the host monolayer and the guest molecules (e.g., adamantane[131–133,137,139,142] and ferrocene derivatives[136,142]) provide a basis for tuning the binding strength with the printboard interface. Multivalent host–guest interactions have been used to tune the binding strength and dynamics on the printboard platform.[137] Nanoscale patterns have also been written and erased on molecular printboard interfaces[132] using microcontact printing[133,142] and DPN[132,133,137] techniques.

Thompson and co-workers[69] have developed a non-covalent, CD-based symmetric templating interface similar to the molecular printboard architecture that is designed to serve four purposes in promoting protein crystallization by (1) concentrating the protein at the interface to achieve local supersaturation, (2) orienting the protein with respect to the CD interface, (3) adsorbing the protein onto the interface via weak, non-covalent interactions that bias the formation of protein crystals due to relatively stronger protein–protein interactions, and (4) presentation of a structured interface to the protein solution that may encourage the propagation of crystal growth into the third dimension via epitaxy (Figure 25). Additional advantages are provided by this non-covalent based approach. For example, the interaction strength and dynamics between the guest–NTA chelating ligand and the cyclodextrin host molecules are structure-dependent, and therefore, tunable based on the selection of the host–guest partners. In this non-covalent amphiphile approach, cyclo-

dextrin derivatives that have been acylated on the primary 6-hydroxymethyl rim of the CD are used as the host matrix and lysine NTA moieties are used as the guest ligands (Table 3 and Figures 9 and 10). Since there is a great diversity of known host–guest stability constants that offer differences in binding that vary by over four orders of magnitude for various host–guest pairs,[143,144] this approach is amenable to high-throughput screening approaches to identify the appropriate conditions for nucleation and growth of protein crystals. Furthermore, the highly symmetric nature of the CD template interface may be capable of propagating order from molecular to mesoscopic length scales, leading to the epitaxial growth of his_6-tag protein crystals from the nanostructured interfacial template.

♦ Summary and Outlook

After experiencing a period of rapid development in the 1990's, progress in the field of interfacial protein crystallization has slowed in recent years, largely due to the dearth of materials that are available to affect the crystallization process and the complexity of controlling nucleation and crystal growth conditions with the available lipid materials. The development of highly symmetric scaffold interfaces that overcome these limitations by using a non-covalent interaction between the protein and the lipid interface whose strength can be tuned to vary the rate of protein docking and migration along lipid monolayer is one method that may favor 2D protein crystallization by allowing protein–protein contacts to govern crystal packing. This approach provides a mechanism for protein crystal self-organization and self-correction via reversible molecular recognition events at the host–guest interface so that the crystallization process is not limited by the properties of the protein:Ni^{2+}–lipid complex. The work of Mirkin et al.[129] suggests that protein crystal growth may be controllable by utilizing highly periodic substrates as nucleation templates and localized flow to the template as a means to control crystal growth rates. Data derived from microfluidics experiments provide further evidence that control over protein crystallization can be obtained by manipulating the timing of nucleation and crystal growth processes.[12–15,125–128] The extensive and growing number of proteins that have been crystallized using the interfacial templating approach suggests that this method still offers great promise for medium resolution structural biological applications. Taken together, it seems reasonable to expect that interfacial templating of protein crystallization can emerge as an even more powerful tool for high-throughput structure analysis, particularly if universal, rapid and rational methods for templating protein crystallization in a predictable manner can be developed.

♦ Acknowledgement

The authors gratefully acknowledge the support of NIH GM079058.

References

1 H. B. Woodruff, R. W. Burg, "Discoveries in Pharmacology" Elsevier, New York, NY, (1986), Vol. 3, p. 338.
2 T. G. Geary, *Trends Parasitol.* **2005**, *21*, 530.
3 R. Capdeville, E. Buchdunger, J. Zimmermann, A. Matter, *Nat. Rev. Drug Disc.* **2002**, *1*, 493.
4 N. R. Taylor, A. Cleasby, O. Singh, T. Skarzynski, A. J. Wonacott, P. W. Smith, S. L. Sollis, P. D. Howes, P. C. Cherry, R. Bethell, P. Colman, J. Varghese, *J. Med. Chem.* **1998**, *41*, 798.
5 J. C. Dyason, M. von Itzstein, *Aust. J. Chem.* **2001**, *54*, 663.
6 A. McPherson, *Methods* **2004**, *34*, 254.
7 N. Asherie, *Methods* **2004**, *34*, 266.
8 N. E. Chayen, *Prog. Biophys. Mol. Biol.* **2005**, *88*, 329.
9 C. F. Snook, M. D. Purdy, M. C. Wiener, *J. Appl. Crystallogr.* **2000**, *33*, 344.
10 D. Stock, O. Perisic, J. Löwe, *Prog. Biophys. Mol. Biol.* **2005**, *88*, 311.
11 M. L. Pusey, Z.-J. Liu, W. Tempel, J. Praissman, D. Lin, B.-C. Wang, J. A. Gavira, J. D. Ng, *Prog. Biophys. Mol. Biol.* **2005**, *88*, 359.
12 B. Zheng, L. S. Roach, R. F. Ismagilov, *J. Am. Chem. Soc.* **2003**, *125*, 11170.
13 B. Zheng, J. D. Tice, L. S. Roach, R. F. Ismagilov, *Angew. Chem., Int. Ed.* **2004**, *43*, 2508.
14 B. Zheng, C. J. Gerdts, R. F. Ismagilov, *Curr. Opin. Struct. Biol.* **2005**, *15*, 548.
15 S. Talreja, D. Y. Kim, A. Y. Mirarefi, C. F. Zukoski, P. J. A. Kenis, *J. Appl. Crystallogr.* **2005**, *38*, 988.
16 J. Jancarik, S.-H. Kim, *J. Appl. Crystallogr.* **1991**, *24*, 409.
17 B. Rupp, *Acc. Chem. Res.* **2003**, *36*, 173.
18 A. George, W. W. Wilson, *Acta Cryst. D* **1994**, *50*, 361.
19 D. F. Rosenbaum, A. Kulkarni, S. Ramakrishnan, C. F. Zukoski, *J. Chem. Phys.* **1999**, *111*, 9882.
20 B. L. Neal, D. Asthagiri, O. D. Velev, A. M. Lenhoff, E. W. Kaler, *J. Cryst. Growth* **1999**, *196*, 377.
21 F. Bonneté, S. Finet, A. Tardieu, *J. Cryst. Growth* **1999**, *196*, 403.
22 J. Narayanan, X. Y. Liu, *Biophys. J.* **2003**, *84*, 523.
23 D.-W. Zhu, A. Garneau, M. Mazumdar, M. Zhou, G.-J. Xu, S.-X. Lin, *J. Struct. Biol.* **2006**, *154*, 297.
24 Y. Jia, X.-Y. Liu, *J. Phys. Chem. B* **2006**, *110*, 6949.
25 E. Barklis, J. McDermott, S. Wilkens, S. Fuller, D. H. Thompson, *J. Biol. Chem.* **1998**, *273*, 7177.
26 C. Vénien-Bryan, P.-F. Lenné, C. Zakri, A. Renault, A. Brisson, J.-F. Legrand, B. Berge, *Biophys. J.* **1998**, *74*, 2649.
27 L. Lebeau, S. Nuss, P. Schultz, P. Oudet, C. Mioskowski, *Chem. Phys. Lipids* **1999**, *103*, 37.
28 S. Nuss, C. Mioskowski, L. Lebeau, *Chem. Phys. Lipids* **1999**, *103*, 21.
29 F. J. Asturias, R. D. Kornberg, *J. Biol. Chem.* **1999**, *274*, 6813.
30 E. E. Uzgiris, R. D. Kornberg, *Nature* **1983**, *301*, 125.
31 A. M. Edwards, S. A. Darst, W. J. Feaver, N. E. Thompson, R. R. Burgess, R. D. Kornberg, *Proc. Natl. Acad. Sci. U.S.A.* **1990**, *87*, 2122.
32 P. Schultz, H. Célia, M. Riva, S. A. Darst, P. Colin, R. D. Kornberg, A. Sentenac, P. Oudet, *J. Mol. Biol.* **1990**, *216*, 353.
33 S. A. Darst, A. M. Edwards, E. W. Kubalek, R. D. Kornberg, *Cell* **1991**, *66*, 121.
34 P. Cramer, D. A. Bushnell, R. D. Kornberg, *Science* **2001**, *292*, 1863.
35 P. Cramer, D. A. Bushnell, J. Fu, A. L. Gnatt, B. Maier-Davis, N. E. Thompson, R. R. Burgess, A. M. Edwards, P. R. David, R. D. Kornberg, *Science* **2000**, *288*, 640.

36 S. A. Darst, M. Ahlers, P. H. Meller, E. W. Kubalek, R. Blankenburg, H. O. Ribi, H. Ringsdorf, R. D. Kornberg, *Biophys. J.* **1991**, *59*, 387.
37 A. C. Ku, S. A. Darst, R. D. Kornberg, C. R. Robertson, A. P. Gast, *Langmuir* **1992**, *8*, 2357.
38 J. Spinke, M. Liley, H. Guder, L. Angermaier, W. Knoll, *Langmuir* **1993**, *9*, 1821.
39 A. C. Ku, S. A. Darst, C. R. Robertson, A. P. Gast, R. D. Kornberg, *J. Phys. Chem.* **1993**, *97*, 3013.
40 S. A. Hemming, A. Bochkarev, S. A. Darst, R. D. Kornberg, P. Ala, D. S. C. Yang, A. M. Edwards, *J. Mol. Biol.* **1995**, *246*, 308.
41 A. J. Avila-Sakar, W. Chiu, *Biophys. J.* **1996**, *70*, 57.
42 L. Lebeau, E. Regnier, P. Schultz, J. C. Wang, C. Mioskowski, P. Oudet, *FEBS Lett.* **1990**, *267*, 38.
43 H. Celia, L. Hoermann, P. Schultz, L. Lebeau, V. Mallouh, D. B. Wigley, J. C. Wang, C. Mioskowski, P. Oudet, *J. Mol. Biol.* **1994**, *236*, 618.
44 L. Schmitt, R. Tampé, *J. Am. Chem. Soc.* **1996**, *118*, 5532.
45 E. E. Uzgiris, *Biochem. Biophys. Res. Commun.* **1986**, *134*, 819.
46 J. Porath, J. Carlsson, I. Olsson, G. Belfrage, *Nature* **1975**, *258*, 598.
47 E. Hochuli, H. Dobeli, A. Schacher, *J. Chromatogr., A* **1987**, *411*, 177.
48 I. T. Dorn, K. Pawlitschko, S. C. Pettinger, R. Tampé, *Biol. Chem.* **1998**, *379*, 1151.
49 E. Gizeli, J. Glad, *Anal. Chem.* **2004**, *76*, 3995.
50 C. I. N. Ayudhya, V. Prachayasittikul, H.-J. Galla, *Eur. Biophys. J.* **2004**, *33*, 522.
51 V. Prachayasittikul, C. I. N. Ayudhya, L. Hilterhaus, A. Hinz, T. Tantimongcolwat, H.-J. Galla, *Biochem. Biophys. Res. Commun.* **2005**, *327*, 174.
52 J. Schmitt, H. Hess, H. G. Stunnenberg, *Mol. Biol. Rep.* **1993**, *18*, 223.
53 T. Stora, R. Hovius, Z. Dienes, M. Pachoud, H. Vogel, *Langmuir* **1997**, *13*, 5211.
54 D. Tareste, F. Pincet, M. Brellier, C. Mioskowski, É. Perez, *J. Am. Chem. Soc.* **2005**, *127*, 3879.
55 W. Frey, W. R. Schief, D. W. Pack, C.-T. Chen, A. Chilkoti, P. Stayton, V. Vogel, F. H. Arnold, *Proc. Natl. Acad. Sci. U.S.A.* **1996**, *93*, 4937.
56 L. Schmitt, C. Dietrich, R. Tampé, *J. Am. Chem. Soc.* **1994**, *116*, 8485.
57 E. W. Kubalek, S. F. J. L. Grice, P. O. Brown, *J. Struct. Biol.* **1994**, *113*, 117.
58 I. T. Dorn, K. R. Neumaier, R. Tampé, *J. Am. Chem. Soc.* **1998**, *120*, 2753.
59 I. T. Dorn, U. G. Hofmann, J. Peltonen, R. Tampé, *Langmuir* **1998**, *14*, 4836.
60 E. M. Wilson-Kubalek, R. E. Brown, H. Celia, R. A. Milligan, *Proc. Natl. Acad. Sci. U.S.A.* **1998**, *95*, 8040.
61 E. Barklis, J. McDermott, S. Wilkens, E. Schabtach, M. F. Schmid, S. Fuller, S. Karanjia, Z. Love, R. Jones, Y. Rui, X. Zhao, D. H. Thompson, *EMBO J.* **1997**, *16*, 1199.
62 C. Vénien-Bryan, F. Balavoine, B. Toussaint, C. Mioskowski, E. A. Hewat, B. Helme, P. M. Vignais, *J. Mol. Biol.* **1997**, *274*, 687.
63 N. Bischler, F. Balavoine, P. Milkereit, H. Tschochner, C. Mioskowski, P. Schultz, *Biophys. J.* **1998**, *74*, 1522.
64 S. Courty, L. Lebeau, L. Martel, P.-F. Lenné, F. Balavoine, W. Dischert, O. Konovalov, C. Mioskowski, J.-F. Legrand, C. Ve'nien-Bryan, *Langmuir* **2002**, *18*, 9502.
65 B. C. Roy, S. Mallik, *J. Org. Chem.* **1999**, *64*, 2969.
66 J. G. Altin, M. G. Banwell, P. A. Coghlan, C. J. Easton, M. R. Nairn, D. A. Offermann, *Aust. J. Chem.* **2006**, *59*, 302.
67 Z. Huang, J. I. Park, D. S. Watson, P. Hwang, F. C. Szoka, *Bioconjugate Chem.* **2006**, *17*, 1592.
68 M. Kellermann, W. Bauer, A. Hirsch, B. Schade, K. Ludwig, C. Bottcher, *Angew. Chem., Int. Ed.* **2004**, *43*, 2959.
69 M. Zhou, S. Haldar, J. Franses, J.-M. Kim, D. H. Thompson, *Supramol. Chem.* **2005**, *17*, 101.
70 D. R. Shnek, D. W. Pack, D. Y. Sasaki, F. H. Arnold, *Langmuir* **1994**, *10*, 2382.
71 D. W. Pack, G. Chen, K. M. Maloney, C.-T. Chen, F. H. Arnold, *J. Am. Chem. Soc.* **1997**, *119*, 2479.
72 K. Ng, D. W. Pack, D. Y. Sasaki, F. H. Arnold, *Langmuir* **1995**, *11*, 4048.
73 S. W. Jeong, D. F. O'Brien, *J. Org. Chem.* **2001**, *66*, 4799.
74 B. C. Roy, R. Peterson, S. Mallik, A. D. Campiglia, *J. Org. Chem.* **2000**, *65*, 3644.
75 C. Dietrich, L. Schmitt, R. Tampe, *Proc. Natl. Acad. Sci. U.S.A.* **1995**, *92*, 9014.
76 S. Gritsch, K. Neumaier, L. Schmitt, R. Tampe, *Biosens. Bioelectron.* **1995**, *10*, 805.
77 B. Carragher, N. Kisseberth, D. Kriegman, R. A. Milligan, C. S. Potter, J. Pulokas, A. Reilein, *J. Struct. Biol.* **2000**, *132*, 33.
78 R. Blankenburg, P. Meller, H. Ringsdorf, C. Salesse, *Biochemistry* **1989**, *28*, 8214.
79 T. L. Calvert, D. Leckband, *Langmuir* **1997**, *13*, 6737.
80 S.-W. Wang, C. R. Robertson, A. Gast, *J. Phys. Chem. B* **1999**, *103*, 7751.
81 S.-W. Wang, C. Robertson, A. Gast, S. Koppenol, T. Edwards, V. Vogel, P. Stayton, *Langmuir* **2000**, *16*, 5199.
82 P. Ratanabanangkoon, A. P. Gast, *Langmuir* **2003**, *19*, 1794.
83 D. Pum, M. Weinhandl, C. Hodl, U. B. Sleytr, *J. Bacteriol.* **1993**, *175*, 2762.
84 D. Pum, U. B. Sleytr, *Thin Solid Films* **1994**, *244*, 882.
85 J. F. Nomellini, S. Kupcu, U. B. Sleytr, J. Smit, *J. Bacteriol.* **1997**, *179*, 6349.
86 M. Weygand, B. Wetzer, D. Pum, U. B. Sleytr, N. Cuvillier, K. Kjaer, P. B. Howes, M. Lösche, *Biophys. J.* **1999**, *76*, 458.
87 U. B. Sleytr, E. Györvary, D. Pum, *Prog. Org. Coating* **2003**, *47*, 279.
88 J. Martin-Benito, F. Gavilanes, V. de los Rios, J. M. Mancheño, J. J. Fernández, J. G. Gavilanes, *Biophys. J.* **2000**, *78*, 3186.
89 F. Oling, W. Bergsma-Schutter, A. Brisson, *J. Struct. Biol.* **2001**, *133*, 55.
90 I. Reviakine, W. Bergsma-Schutter, A. N. Morozov, A. Brisson, *Langmuir* **2001**, *17*, 1680.
91 H.-W. Wang, S.-F. Sui, *J. Struct. Biol.* **2001**, *134*, 46.
92 X. Hagnerelle, C. Plisson, O. Lambert, S. Marco, J. L. Rigaud, L. Johannes, D. Lévy, *J. Struct. Biol.* **2002**, *139*,

113.
93 Y. Chen, Y.-J. Lu, H.-W. Wang, S. Quan, Z. Chang, S.-F. Sui, *Biochem. Biophys. Res. Commun.* **2003**, *310*, 360.
94 A. M. Makhov, D. W. Taylor, J. D. Griffith, *Biochim. Biophys. Acta* **2004**, *1701*, 101.
95 W. Frey, J. Brink, W. R. Schief, W. Chiu, V. Vogel, *Biophys. J.* **1998**, *74*, 2674.
96 V. Vogel, W. R. Schief, W. Frey, *Supramol. Sci.* **1997**, *4*, 163.
97 W. R. Schief, S. R. Dennis, W. Frey, V. Vogel, *Coll. Surf., A* **2000**, *171*, 75.
98 S. A. Darst, A. M. Edwards, *Curr. Opin. Struct. Biol.* **1995**, *5*, 640.
99 V. Prachayasittikul, C. I. N. Ayudhya, T. Tantimongcolwat, H.-J. Galla, *Biochem. Biophys. Res. Commun.* **2005**, *326*, 298.
100 G. Zuber, E. Barklis, *Biophys. J.* **2000**, *78*, 373.
101 J. McDermott, K. Mayo, E. Barklis, *J. Mol. Biol.* **2000**, *302*, 121.
102 B. K. Ganser, A. Cheng, W. I. Sundquist, M. Yeager, *EMBO J.* **2003**, *22*, 2886.
103 K. Mayo, M. L. Vana, J. McDermott, D. Huseby, J. Leis, E. Barklis, *J. Mol. Biol.* **2002**, *316*, 667.
104 A. J. Avila-Sakar, S. Misaghi, E. M. Wilson-Kubalek, K. H. Downing, H. Zgurskaya, H. Nikaido, E. Nogales, *J. Struct. Biol.* **2001**, *136*, 81.
105 F. Kienberger, R. Moser, H. Schindler, D. Blaas, P. Hinterdorfer, *Single Mol.* **2001**, *2*, 99.
106 A. Thess, S. Hutschenreiter, M. Hofmann, R. Tampé, W. Baumeister, R. Guckenberger, *J. Biol. Chem.* **2002**, *277*, 36321.
107 C. M. Hill, I. R. Bates, G. F. White, F. R. Hallett, G. Harauz, *J. Struct. Biol.* **2002**, *139*, 13.
108 G. G. Chikh, W. M. Li, M.-P. Schutze-Redelmeier, J.-C. Meunier, M. B. Bally, *Biochim. Biophys. Acta* **2002**, *1567*, 204.
109 C. L. van Broekhoven, J. G. Altin, *Int. J. Cancer* **2002**, *98*, 63.
110 C. L. van Broekhoven, J. G. Altin, *Biochim. Biophys. Acta* **2005**, *1716*, 104.
111 S. Lata, J. Piehler, *Anal. Chem.* **2005**, *77*, 1096.
112 S. Lata, A. Reichel, R. Brock, R. Tampé, J. Piehler, *J. Am. Chem. Soc.* **2005**, *127*, 10205.
113 T. X. Dang, E. M. Hotze, I. Rouiller, R. K. Tweten, E. M. Wilson-Kubalek, *J. Struct. Biol.* **2005**, *150*, 100.
114 D. W. Schuerch, E. M. Wilson-Kubalek, R. K. Tweten, *Proc. Natl. Acad. Sci. U.S.A.* **2005**, *102*, 12537.
115 T. X. Dang, R. A. Milligan, R. K. Tweten, E. M. Wilson-Kubalek, *J. Struct. Biol.* **2005**, *152*, 129.
116 T. X. Dang, S. J. Farah, A. Gast, C. Robertson, B. Carragher, E. Egelman, E. M. Wilson-Kubalek, *J. Struct. Biol.* **2005**, *150*, 90.
117 C. Richard, F. Balavoine, P. Schultz, T. W. Ebbesen, C. Mioskowski, *Science* **2003**, *300*, 775.
118 S. Subramaniam, J. L. S. Milne, *Annu. Rev. Biophys. Biomol. Struct.* **2004**, *33*, 141.
119 E. W. Kubalek, R. D. Kornberg, S. A. Darst, *Ultramicroscopy* **1991**, *35*, 295.
120 F. J. Asturias, R. D. Kornberg, *J. Struct. Biol.* **1995**, *114*, 60.
121 L. Lebeau, F. Lach, C. Vénien-Bryan, A. Renault, J. Dietrich, T. Jahn, M. G. Palmgren, W. Kühlbrandt, C. Mioskowski, *J. Mol. Biol.* **2001**, *308*, 639.
122 R. P. Richter, J. L. K. Him, B. Tessier, C. Tessier, A. R. Brisson, *Biophys. J.* **2005**, *89*, 3372.
123 J.-M. Altenburger, L. Lebeau, C. Mioskowski, D. Schirlin, *Helv. Chim. Acta* **1992**, *75*, 2538.
124 E. Trudel, J. Gallant, S. Mons, C. Mioskowski, L. Lebeau, K. Jeuris, P. Foubert, F. De Schryver, C. Salesse, *Biophys. J.* **2001**, *81*, 563.
125 G. He, V. Bhamidi, S. R. Wilson, R. B. H. Tan, P. J. A. Kenis, C. F. Zukoski, *Cryst. Growth Design* **2006**, *6*, 1746.
126 D. L. Chen, C. J. Gerdts, R. F. Ismagilov, *J. Am. Chem. Soc.* **2005**, *127*, 9672.
127 H. Song, D. L. Chen, R. F. Ismagilov, *Angew. Chem., Int. Ed.* **2006**, *45*, 7336.
128 C. J. Gerdts, V. Tereshko, M. K. Yadav, I. Dementieva, F. Collart, A. Joachimiak, R. C. Stevens, P. Kuhn, A. Kossiakoff, R. F. Ismagilov, *Angew. Chem., Int. Ed.* **2006**, *45*, 8156.
129 X. Liu, Y. Zhang, D. K. Goswami, J. S. Okasinski, K. Salaita, P. Sun, M. J. Bedzyk, C. A. Mirkin, *Science* **2005**, *307*, 1763.
130 B. J. Ravoo, R. Darcy, *Angew. Chem.* **2000**, *39*, 4324.
131 J. Huskens, M. A. Deij, D. N. Reinhoudt, *Angew. Chem., Int. Ed.* **2002**, *41*, 4467.
132 T. Auletta, B. Dordi, A. Mulder, A. Sartori, S. Onclin, C. M. Bruinink, M. Péter, C. A. Nijhuis, H. Beijleveld, H. Schonherr, G. J. Vancso, A. Casnati, R. Ungaro, B. J. Ravoo, J. Huskens, D. N. Reinhoudt, *Angew. Chem., Int. Ed.* **2004**, *43*, 369.
133 C. M. Bruinink, C. A. Nijhuis, M. Péter, B. Dordi, O. Crespo-Biel, T. Auletta, A. Mulder, H. Schonherr, G. J. Vancso, J. Huskens, D. N. Reinhoudt, *Chem.—Eur. J.* **2005**, *11*, 3988.
134 S. Onclin, A. Mulder, J. Huskens, B. J. Ravoo, D. N. Reinhoudt, *Langmuir* **2004**, *20*, 5460.
135 V. Mahalingam, S. Onclin, M. Péter, B. J. Ravoo, J. Huskens, D. N. Reinhoudt, *Langmuir* **2004**, *20*, 11756.
136 C. A. Nijhuis, J. Huskens, D. N, Reinhoudt, *J. Am. Chem. Soc.* **2004**, *126*, 12266.
137 A. Mulder, S. Onclin, M. Péter, J. P. Hoogenboom, H. Beijleveld, J. Maat, M. F. Carcía-Parajó, B. J. Ravoo, J. Huskens, N. F. Hulst, D. N. Reinhoudt, *Small* **2005**, *1*, 242.
138 J. Huskens, A. Mulder, T. Auletta, C. A. Nijhuis, M. J. W. Ludden, D. N. Reinhoudt, *J. Am. Chem. Soc.* **2004**, *126*, 6784.
139 F. Corbellini, A. Mulder, A. Sartori, M. J. W. Ludden, A. Casnati, R. Ungaro, J. Huskens, M. Crego-Calama, D. N. Reinhoudt, *J. Am. Chem. Soc.* **2004**, *126*, 17050.
140 Y. Tanaka, M. Miyachi, Y. Kobuke, *Angew. Chem., Int. Ed.* **1999**, *38*, 504.
141 M. Strobel, K. Kita-Tokarczyk, A. Taubert, C. Verbert, P. A. Heiney, M. Chami, W. Meier, *Adv. Funct. Mat.* **2006**, *16*, 252.
142 S. Onclin, J. Huskens, B. J. Ravoo, D. N. Reinhoudt, *Small* **2005**, *1*, 852.
143 K. A. Connors, *Chem. Rev.* **1997**, *97*, 1325.
144 M. V. Rekharsky, Y. Inoue, *Chem. Rev.* **1998**, *98*, 1875.